THEORY AND EXPERIMENT OF A NON-RADIATIVE WIRELESS POWER TRANSFER METHOD FOR A LANE MOVING ROBOT

A Thesis

by

Mete Çeşmeci

Submitted to the
Graduate School of Sciences and Engineering
In Partial Fulfillment of the Requirements for
the Degree of

Master of Science

in the
Department of Electrical and Electronics Engineering

Özyeğin University
August 2022

Copyright © 2022 by Mete Çeşmeci

THEORY AND EXPERIMENT OF A NON-RADIATIVE WIRELESS POWER TRANSFER METHOD FOR A LANE MOVING ROBOT

Approved by:

Assistant Professor Göktürk Poyrazoğlu,
Advisor
Department of Electrical and Electronics Engineering
Özyeğin University

Professor Belgin Emre Türkay
Department of Electrical Engineering
İstanbul Technical University

Assistant Professor Kadir Durak
Department of Electrical and Electronics Engineering
Özyeğin University

Date Approved: 11 August 2022

To my mother and my father...

ABSTRACT

Today, the usage of robots is growing in the warehouses for automated organizing of goods and in the field for harvesting foods and other agriculture tasks. Many big resellers use robots in their distribution warehouses in an automated delivery system and, many manufacturers use them in their factories to transfer goods and components between production lines and warehouses integrated with enterprise resource planning (ERP) systems. A battery is needed such devices and, the battery size and capacity needed in such devices can be reduced thanks to WPT technology. It is useful for reducing environmental pollution resulted from disposing of batteries used for battery-operated vehicles and robots. With motivation for reducing battery size in robots, the main aim of the research is to find an alternative method of dynamic wireless power transfer to a moving object such as an electric vehicle or a robot that it moves on wheels on the floor. The well-known systems and their common series-connected/switched road embedded segment structures are discussed and challenged. Then, an alternative method of synchronization to the secondary resonance is presented. The suggested method eliminates switches between road-embedded coil units and makes the energy transition easy among units. This method shortens the length of the EMF radiative part of road embedded segments and the application is suitable for two-dimensional floor embedded structures for robot applications. The experimental and the simulation results are shared. The last chapter concludes thesis with discussion on the results of the thesis and future work.

ÖZETÇE

Günümüzde, depolarda ürünlerin otomatik olarak organize edilmesi, tarım işleri ve gıdaların hasat edilmesi için robotların kullanımı artmaktadır. Birçok büyük dağıtım şirketinin depolarında otomatik bir dağıtım sisteminde robotlar kullanılmaktadır. Birçok üreticinin fabrikalarında malları ve malzemeleri üretim ile depolar arasında aktarmak için ERP sistemleriyle entegre robotlar kullanılmaktadır. Bu tür cihazlarda bataryaya ihtiyaç vardır ve dinamik kablosuz güç transfer (wireless power transfer - WPT) teknolojisi ile ihtiyaç duyulan batarya boyutu ve kapasitesi azaltılabilir. Ömrü biten bataryaların atılmasından kaynaklanan çevre kirliliğini azaltmak için fayda sağlayabilir. Robotlarda batarya boyutunu küçültme motivasyonuyla yapılan bu araştırmanın temel amacı, elektrikli araç veya zemin yüzünde tekerlekler üzerinde hareket eden bir robot gibi hareketli bir nesneye alternatif bir dinamik kablosuz güç aktarımı yöntemi bulmaktır. İyi bilinen sistemler ve bunların ortak seri bağlantılı ara güç anahtarlı yola gömülü segment yapıları tartışılmakta ve irdelenmektedir. Ardından, alternatif olarak önerilen ikincil rezonansa senkronizasyon yöntemi sunulur. Önerilen yöntem, yola gömülü bobin üniteleri arasındaki anhtarlarla geçişleri ortadan kaldırır ve üniteler arasında geçiş esnasında enerjilendirmeyi kolaylaştırır. Bu yöntem, yola gömülü bölümlerin elektromanyetik bozucu yayan kısmının uzunluğunu kısaltır ve uygulama, robot uygulamaları için iki boyutlu zemin gömülü yapılar için uygundur. Sonrasında simülasyon ve deney sonuçları paylaşılmaktadır. Son bölüm, tezin sonuçları ve gelecekteki çalışmalar hakkında tartışma ile tezi sonlandırmaktadır.

ACKNOWLEDGEMENTS

I would like to thank my advisor Asst. Prof. Gokturk Poyrazoglu for his cooperation and weekly follow-up meetings during my studies. And, I would like to thank Vestel Elektronik A.Ş. for providing such a good university education opportunity to its employees.

TABLE OF CONTENTS

LIST OF TABLES

LIST OF FIGURES

CHAPTER I

INTRODUCTION

Technology has changed human life through the ages. With the Fourth Industrial Revolution, the last of the industrial revolutions we are experiencing today, we met many transformative innovations that were not in our lives before. Electric vehicles (EV), robots, and wireless power transfer (WPT) are the ones we encounter in our daily life. Wireless power transfer includes several technologies to transmit power without wires between the power source and the device. One of those technologies is dynamic wireless power transfer through an electrified roadway to a moving vehicle or a robot. The battery is needed such devices and, with WPT technology it can be reduced in size and capacity. It is useful for reducing environmental pollution resulted from disposing of batteries used for battery-operated vehicles and robots. One of the biggest challenges in our age is creating green technologies for the sake of saving the world, sustainability. The research for finding a useful method to wirelessly power robots while they are moving on the ground would be a starting point.

1.1 Motivation

A well-known method is used to set the maximum power output in transmitter circuits. A coil which is attached to a lamp was used for this. Figure 1 shows such coils. The coil was put nearby the resonance tank coil of the output transistor of the transmitter at a distance of approximately 10mm on the tank coil's axis. The tank coil and the lamp coil reproduce a transformer with air distance between primary and secondary sides of the transformer. Then, the trimmer capacitors were adjusted for maximum brightness on the lamp that brightness represents the output power of the transmitter. So this phenomenon is a type of wireless power transfer and gave the enthusiasm to work on wireless power transfer.

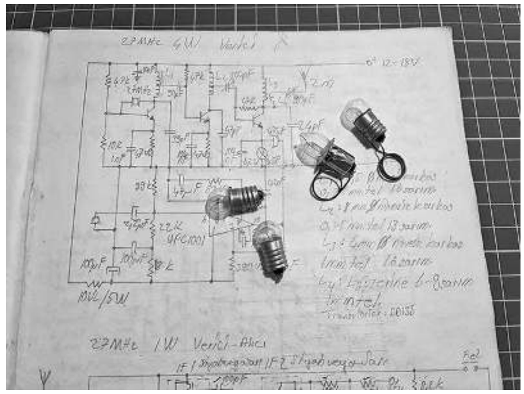

Figure 1: A picture of lamps with coils.

Today, the usage of robots is growing in the warehouses for automated organizing of goods and in the field for harvesting foods and other agriculture tasks. Many big resellers use robots in their distribution warehouses in a computerized delivery system. Many manufacturers use them in their factories to transfer goods and components between production lines and warehouses integrated with ERP systems.

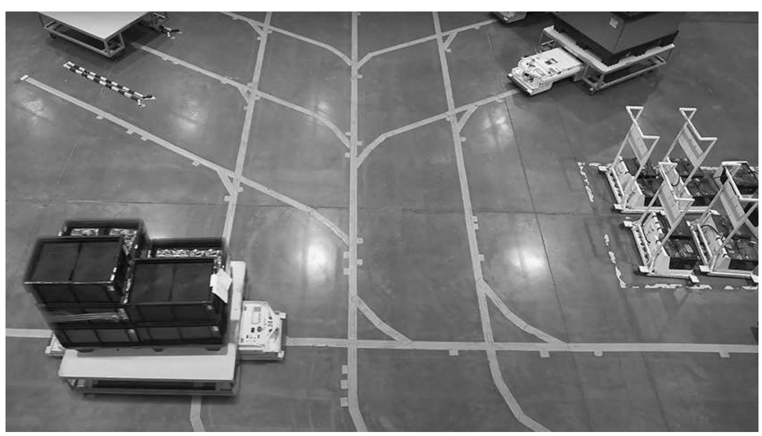

Figure 2: A picture of warehouse robots and their backup battery packs.

Battery packs power these robots. It is needed that some backup batteries must be kept charged and ready to use for quick battery replacement for continuous work in a day. Because one battery pack is not enough for working twenty four hours a day and seven days a week, which is needed in most companies, an example of the robots and the backup battery packs can be seen in Figure 2. In addition to the energy capacity of the battery, the effect of battery weight on the energy consumption during the operation of a robot should be considered during the design of the robot. The total energy expended in a mission of a robot [5] or an EV [6] depends on its total mass and mission time. The robot and the EV must carry their batteries as a part of the primary load weight. By reducing the needed battery capacity, the reliability of EVs and the road range can be increased [7]. Furthermore, to minimize energy usage, the energy consumption of robots needs to be modeled for all complex use cases related to their mission and their dependence on batteries [8], [9]. As a reference of thinking, there are weights for the robots in the study of the MIT team for the MIT Cheetah four-legged robot in 2013 [9] and, the report of the CMU Robotics Institute team for wheeled robots for Mars and Lunar missions in 2014 [5]. Dainis Berjoza and Inara Jurgena have analyzed the effects of the battery weight on electric vehicles and they have shown weights of some EVs and battery packs in their conference paper [10]. Figure 3 shows the findings of this paper. Berjoza and Jurgena also wrote the ratio of the battery weight to the total weight of an EV as a comparison parameter in their other article [11]. They named this ratio as the battery-specific weight coefficient. They have shown the battery-specific weight coefficient varies in range from 0.12 to 0.28 for the same electrical vehicles in Latvia in 2017. The environmental impacts of electric vehicles are important for the sustainability of transportation activities. Amount of used energy, green gas pollution and disposal of hazardous material with batteries at the end of their life cycle are some of them [12]. Increasing trends of usage of dynamic WPT in the EV industry is mentioned by authors as an opportunity for environmental impact of EVs with reducing transport energy consumption through reduction in traction battery mass in their article [13]. Researches are not only on dynamic WPT to EVs but also using charge whenever they stop at traffic intersections for reducing battery mass [14]. From these studies, it can be seen the new methods for reducing battery weight are needed for EVs and robots.

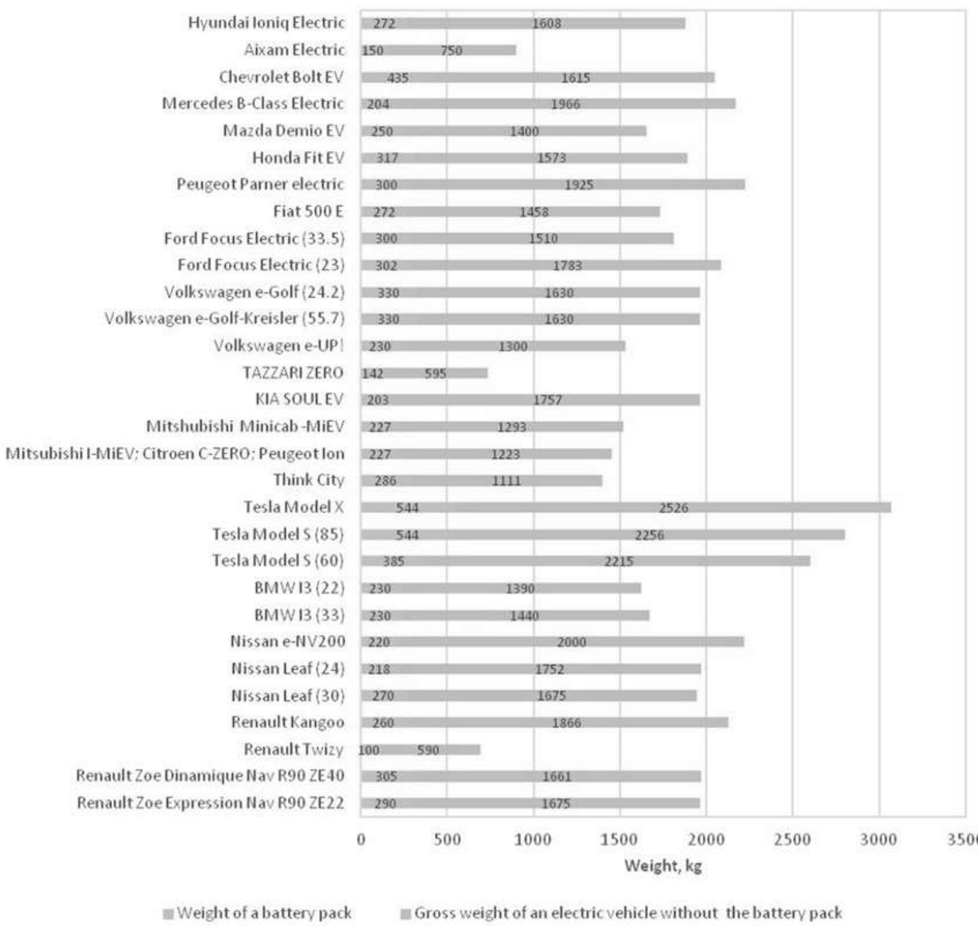

Figure 3: Weights of EVs and their battery packs [6]

A group of researchers from The Polytechnic University of Milan investigated the design of disc formed coils like in Figure 4 in a paper [2]. They shared results of FEM simulations on Ansys Maxwell. Their approach is investigating changes power transferred from primary coil by inductance, by ferrite structure, by gap, by ferrite and copper volume. Their optimization process take in to account power equation shown in Equation 1.

$$P_{out} = Q\omega I_1^2 \frac{M^2}{L} = Q\omega I_1^2 p \quad (1)$$

Where: P_{out} is the output power Q is the resonance factor, $\omega$is the frequency and I_1 is the rms value of the primary current, p is the optimization index [2].

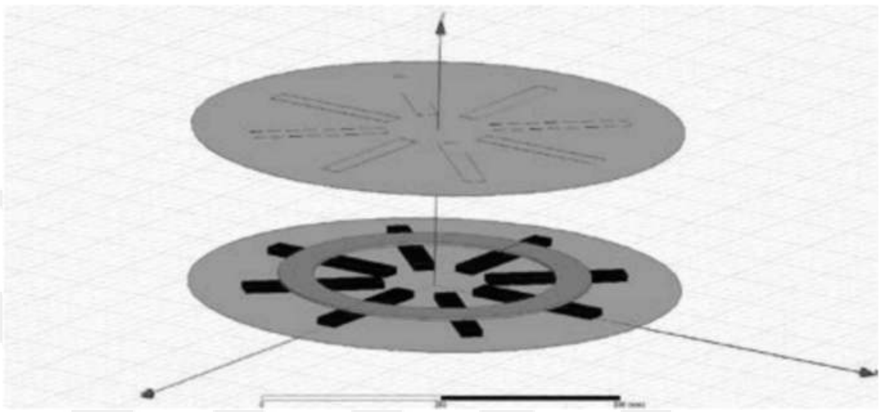

Figure 4: One of the investigated design type of disc coil in the article [2].

The variations of p are investigated related to number of ferrite bars, shape of ferrite bars, length and thickness of ferrite bars by simulations on Maxwell. They also made simulations of ferrite structures added external ring, radial bars, external bars. The results of the simulations shown in Figure 5. The graph in Figure 5 can be interpreted to mean that using one whole ferrite increases the power that can be transferred.

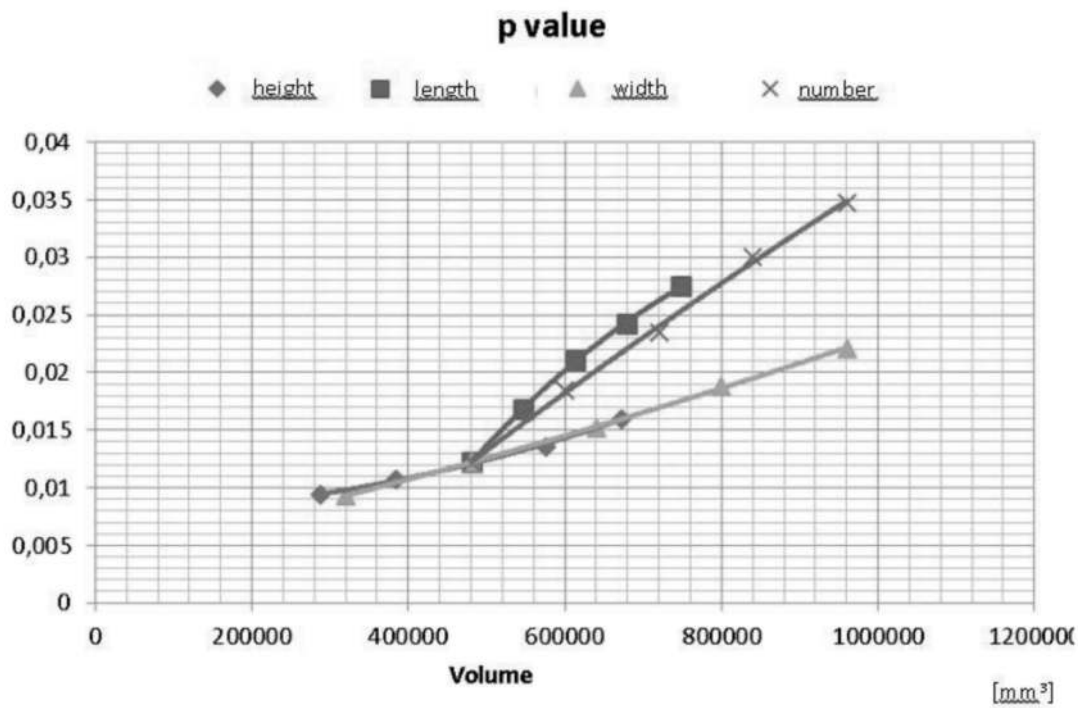

Figure 5: Variation of p with different ferrite bars configuration [2].

1.2 Research Aim, Objectives and Scope

With motivation for reducing battery size in robots, the main aim of the research is to find an alternative method of dynamic wireless power transfer to a moving object such as an electric vehicle or a robot that it moves on wheels on the floor. The well-known systems and their common series-connected/switched road embedded segment structures are discussed and challenged. Then, an alternative method of synchronization to the secondary resonance is presented. The suggested method eliminates switches between road-embedded coil units and makes the energy transition easy among units. This method shortens the length of the EMF radiative part of road embedded segments and the application is suitable for two-dimensional floor embedded structures for robot applications. The experimental and the simulation results are shared.

1.3 Thesis Outline

Other chapters of the thesis are organized as follows. Chapter 2 gives a literature review on wireless power transfer in theory and its classifications. Then, Chapter 3 proposes a new method for robots in moving wireless power transfer. Simulations of the proposed method and their results are presented. The realization and design of the proposed method are shown with the experiment in Chapter 4. A comparison of the simulation and experiment results is presented in Chapter 5. The last chapter concludes the thesis with a discussion on the results of the view and future work.

CHAPTER II

LITERATURE REVIEW

In the early 1800s, Hans Christian Ørsted, André-Marie Ampère, and Michael Faraday discovered the basic laws of electromagnetism. After electromagnetic radiation is discovered by Hertz, Tesla registered his wireless transmitter in a patent, he was the first person to demonstrate the concept of WPT in 1891 [15]. Dynamic inductive WPT for road first patent M. Hutin and M. Leblanc 1894 [16]. After Hutin and Le-Blanc, the EV inductive coupling WPT was forgotten like Tesla's first patent of WPT in 1914 [17]. Professor Don Otto of the University of Auckland in New Zealand proposed an inductively powered vehicle in 1972 using the power generated at 10 kHz [1]. In the 1980s, another WPT project was carried out in California, USA. It was called the Partner for Advanced Transit and Highways (PATH) project [1]. French and German researchers carried out EV-WPT projects known as TULIP (Transport Urban, Individuel et Public – Public and Individual Urban Transport) and Inductive Power Transfer (IPT) respectively in the 1980s and 1990s [1]. Esser and Skudelny published their article in 1991, it was first WPT article for robots [18]. In 2001, Fernandez and Borras granted first battery charger patent [19], [20]. The other recent trend in WPT began with the use of resonant coupling in the United States by the Massachusetts Institute of Technology (MIT) in 2006 [1]. In 2007, Marin Soljacic with a research group at the MIT, presented a non-radiative wireless power transfer system using self-resonance coils. One year later, another research team at Intel reproduced MIT's experiment. By the pressure of increasing usage of a large number of mobile devices such as smartphones, tablets and laptops, the Wireless Power Consortium was founded in 2008. The goal of this association is to establish international standards for standardized wireless charging in the form of the Qi standard [21]. In 2011, Toyota Motor Co. invested in WiTricity Co., one of the first commercial developers of resonant connectivity for wireless power transmission. IHI Co. was given a license from WiTricity Co. in 2011 [1]. Qualcomm published a brochure of their wireless EV charger system "Qualcomm Halo" in the same year. Alliance for Wireless Power (A4WP) to promote resonant coupling WPT, it is established in May 2012 [1]. In 2015, C. T. Rim with a research team at KAIST present an inductive wireless transfer system. In the following years, KAIST teams realized dynamic wireless power transfer systems for powering buses in Korea. In 2019, WiTricity announced the acquisition of Halo from Qualcomm [22].

2.1 Classifications of WPT

There are many classification ways for wireless power transfer (WPT). Basicaly, we can seperate in two type of WPT, one of them is electromagnetic and other non-electromagnetic. In this thesis, non-electromagnetic types are out of scope. Many people have been reviewed WPT systems and circuit topologies [4], [23], [24], [25], [21], [1], [26], [27], [28], [29], [30], [31], [32]. In the light of their studies, we can set out classification related to scope of this thesis. Here is the combination of electromagnetic WPT classifications as a diagram, in Figure 6.

When the power is transferred via a magnetic field, it is called magnetically coupled WPT, inductive coupling WPT, or inductive power transfer (IPT). When the primary side and secondary side are established as resonance circuits, the system is called resonant WPT. Here is the classification diagram for magnetically coupled resonant WPT in Figure 7.

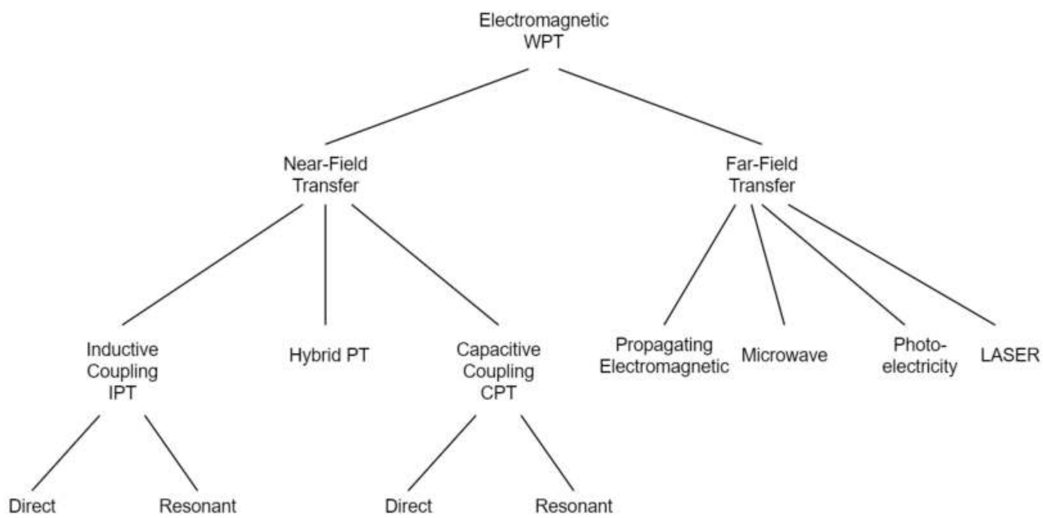

Figure 6: Classification of electromagnetic WPT.

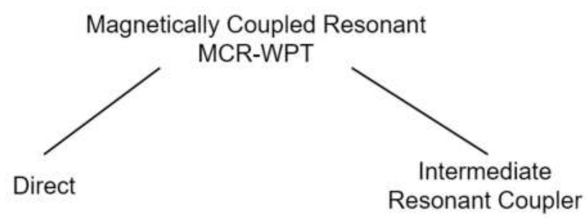

Figure 7: Classification of magnetically coupled resonant WPT.

For the resonant WPT, related to circuit topologies of primary and secondary sides, we can classify the WPT methods as if their circuits are in serial resonance circuits or parallel resonance circuits. Figure 8 shows a classification of WPT according to primary and secondary circuit topologies.

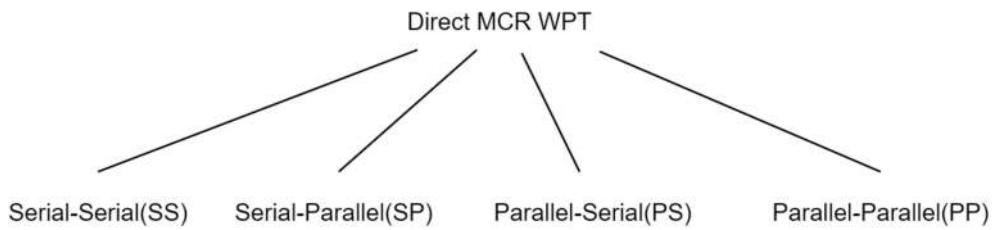

Figure 8: Classification of direct magnetically coupled resonant WPT.

Figure 9 shows a classification made by Yiming Zhang. He showed basic structures of WPT circuits in his doctoral thesis, which Springer Thesis published as Recognizing Outstanding Ph.D. Research [3].

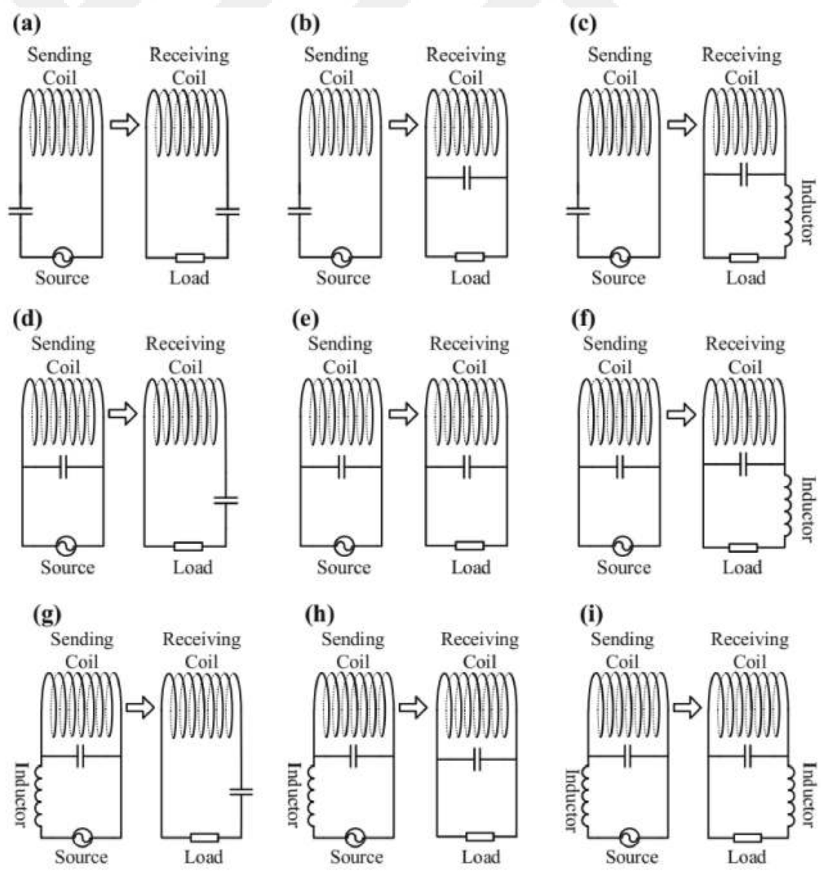

Figure 9: Most common IPT structures: (a) SS; (b) SP; (c) S-LCL; (d) PS; (e) PP; (f) P-LCL; (g) LCL-S; (h) LCL-P; (i) LCL-LCL [3]

Another classification can be related to the distance between the transmitter and receiver coil. Figure 10 shows such classification related to the distance.

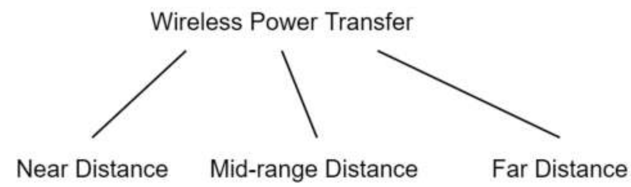

Figure 10: Classification of WPT related to distance between transmitter and receiver coils.

If the coils do not stand still and one of them moves, it is called Dynamic WPT. Figure 11 shows such classification related to the movement.

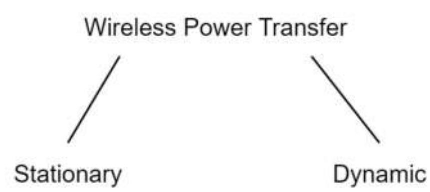

Figure 11: Classification of WPT related to movement of transmitter coil or receiver coil.

There are the most common primary side circuit topologies of a transmitter of a WPT. Figure 12 shows four basic circuit topologies of primary side.

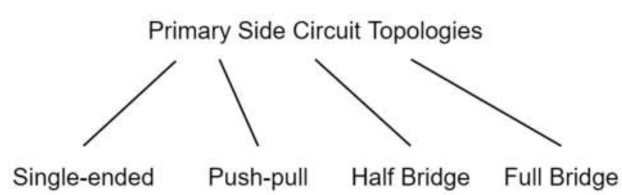

Figure 12: Four basic circuit topologies of primary side.

The transmitter coils may be more than one, and they can be driven with one phase, or each coil can be operated with one of the phases of the multi-phase drive structure [31]. Multi-phase systems can be used to reduce power ripples on the receiver side [33]. Figure 13 shows common structures related to phase count on the transmitter side of the WPT system.

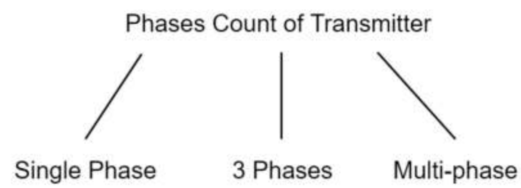

Figure 13: Classification related to phase count on transmitter structure.

Regarding the WPT system's needs, it may use more than one transmitter (TX) coil or transmitters to transfer power to one or more receiver coils (RX) or receivers. Figure 14 shows basic structures of WPT related to transmitter and receiver.

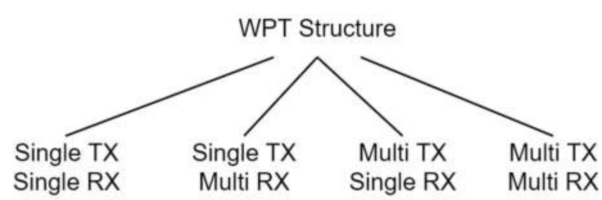

Figure 14: Basic structures of WPT.

The transmitter and receiver are electromagnetically coupled, and energy is transmitted wirelessly via an electric, magnetic, or electromagnetic wave. WPT over radio waves requires higher frequencies, such as microwaves, to effectively focus on wireless performance. Table 1 shows the general characteristics of the various WPT technologies. The main difference between inductively coupled and resonant coupling is the presence of non-resonance and resonance, respectively.

Table 1: Characteristics of WPT technologies as of 2014 [1].

	Via radiowaves	**Resonant coupling**	**Inductive coupling**
Field	Electromangetic	Resonance	Magnetic field
Method	Antenna	Resonator	Coil
Efficiency	Low to high	High	High
Distance	Short to long	Medium	Short
Power	Low to high	High	High
Safety	EM	Under discussion	Magnetic
Regulation	Radiowave	Under discussion	Under discussion

2.2 Non-radiative WPT Systems

Non-radiative WPT Systems are known as near field systems and transfer power through magnetic fields. The coupling devices of the inductive WPT systems are two coils mutually coupled. The transmitting coil is excited by an alternating current at a high frequency, generally between 10kHz and 150kHz. The inductive WPT systems utilize two topologies for transferring power, and the relevant systems are termed inductive coupling, and resonant coupling WPT system [34].

As another example of a non-radiative WPT system, in 2007, Aristeidis Karalis, Andre B. Kurs, Robert Moffatt, John D. Joannopoulos, Peter H. Fisher, and Marin Soljacic from MIT showed a non-radiative mid-range system with intermediate resonance coupler. [35], [36]. Their system demonstrated mid-range wireless power transfer to a 60W light bulb to more than two meters. They granted a patent for their non-radiative system in 2010 [37].

2.3 Theory of Inductive Coupled Resonant WPT

The basic principle of WPT is based on Faraday and Ampere's laws. The principle of wireless power transmission is to generate an induced electromagnetic field by feeding a transmit coil (Tx) connected to a receive coil (Rx) and regenerating the power to feed a load. The coils and the magnetic fluxes created coils themselves Φ_{11}, Φ_{12}, Φ_{22}, Φ_{21} are shown in Figure 15 for no-load case and in Figure 16 for with-load case.

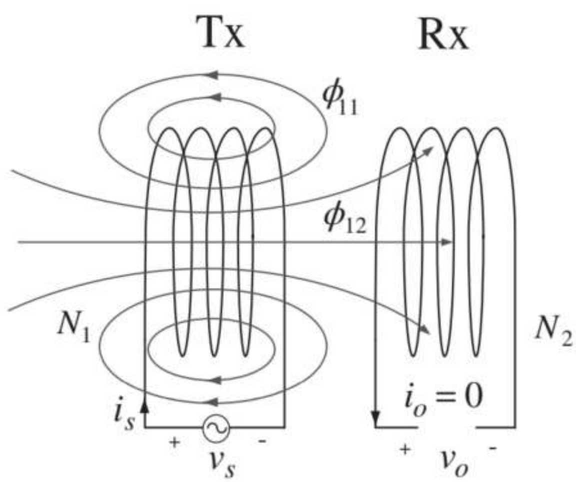

Figure 15: The magnetic flux of the two coupled inductors in the instantaneous time domain. No-load case [4].

During the receiver is loaded, receiver coil creates fluxes Φ_{22} and Φ_{21}, this fluxes induces transmitter coil also. So two coils are not coupled only magnetically but also electrically in most cases. Thus, the load conditions are reflected on the transmitter or the primary side.

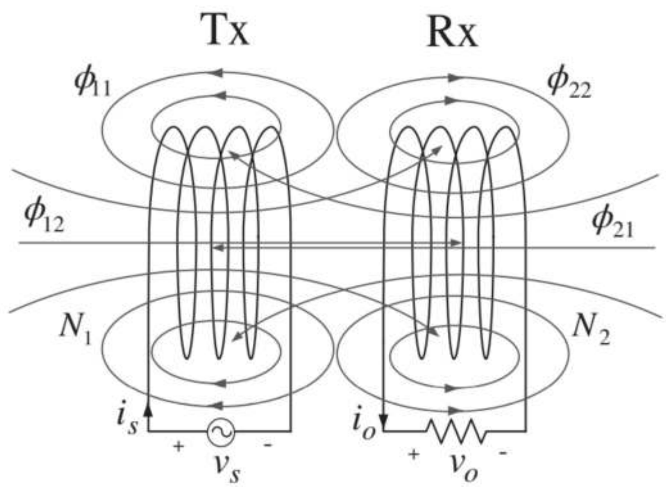

Figure 16: The magnetic flux of the two coupled inductors in the instantaneous time domain. With-load case [4].

The relationship between WPT and Faraday and Ampere laws is shown in Figure 17 with most known equations.

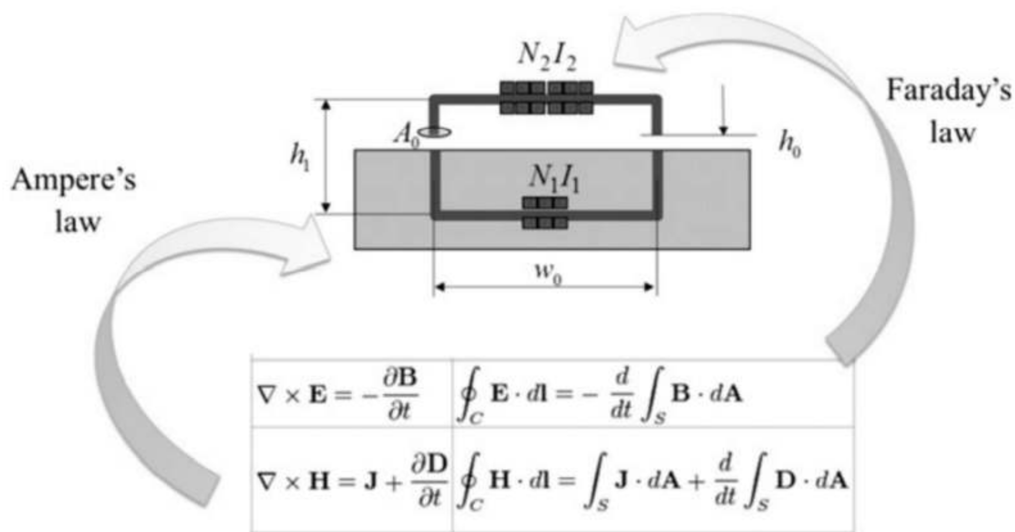

Figure 17: Basic IPT equation in general [4].

In a steady state with a fixed frequency sinusoidal voltage source, phasors can simplify the system and better understand WPT, including compensation elements on both sides. An equivalent circuit of WPT can be seen in Figure 19.

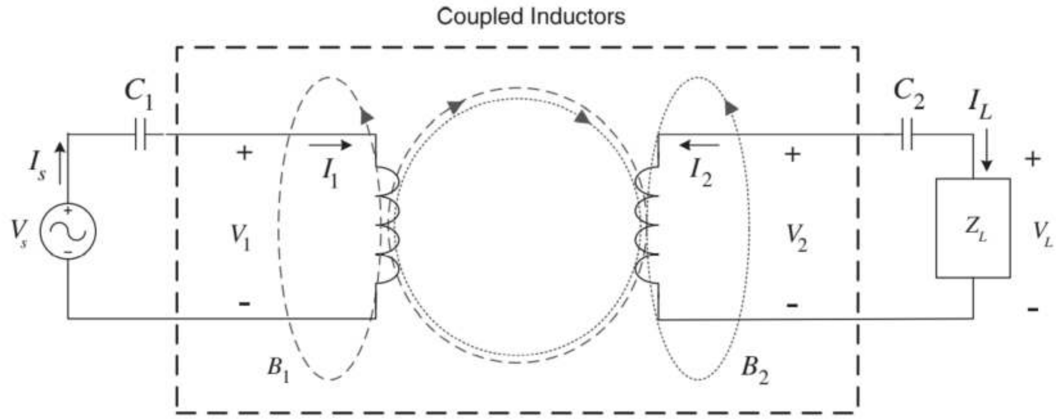

Figure 18: Equivalent circuit of IPT system in phasor domain [4].

Including compensation circuit types on both sides, we can draw the principal circuit of WPT as in Figure 19. L_1 and L_2 represents transmitter and receiver coils respectively. They are coupled, and M is the mutual inductance of coils related to the coupling factor between two coils. The main purpose of compensation circuits is to make the reactive component of the impedance reflect the source zero.

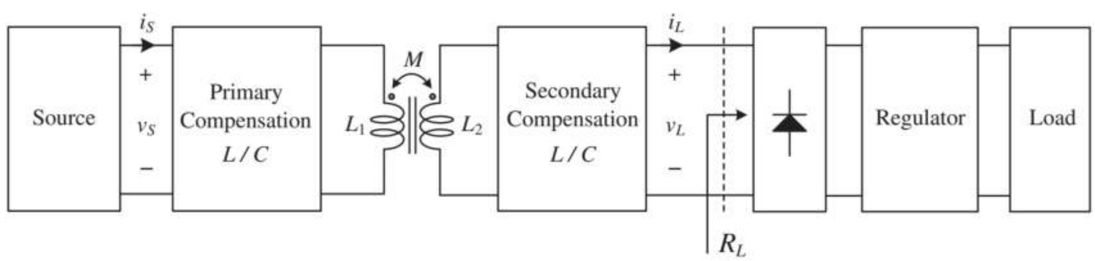

Figure 19: Typical configuration block diagram of inductive WPT compensation circuit [4].

CHAPTER III

SIMULATION OF WPT SYSTEM PROPOSAL FOR MOVING ROBOTS ON THE GROUND

In the light of literature research on dynamic wireless power transfer systems of electric vehicles and robots, a method is proposed that has the properties below:

- Eliminates switches between coil segments or transmit units buried in the road.
- Eliminates latency of communication required to control the energizing of the units.
- Eliminates electromagnetic interference elimination issues seen on long coil structures.

3.1 WPT System Proposal

The main idea of the suggested method may be explained as “the primary tracks the secondary resonance” instead of well-known WPT systems for powering moving objects. Figure 20 shows the basic principle to make this idea real. It is like an oscillator coupled by a transformer to a resonant part. The coupling factor (k3) between the input coil (Lin) and the output coil (Lout) is low enough to prevent self-oscillation. The system does not oscillate if the secondary side (Lres , Cres) exists, but it is not circulating resonant currents. It does not generate a magnetic field that feeds the input coil. If the secondary side exists with its resonant magnetic field, the system takes the input of the resonant field (Lin , Vin). It generates the output magnetic field, which is synchronized to the resonance frequency of the secondary side via (Vout , Lout). It is possible to start the WPT by initial communication for giving frequency value to the system between moving object and supply system during parking mode. If the system is designed for bi-directional WPT, the moving object could generate the initial resonant magnetic field required for start-up.

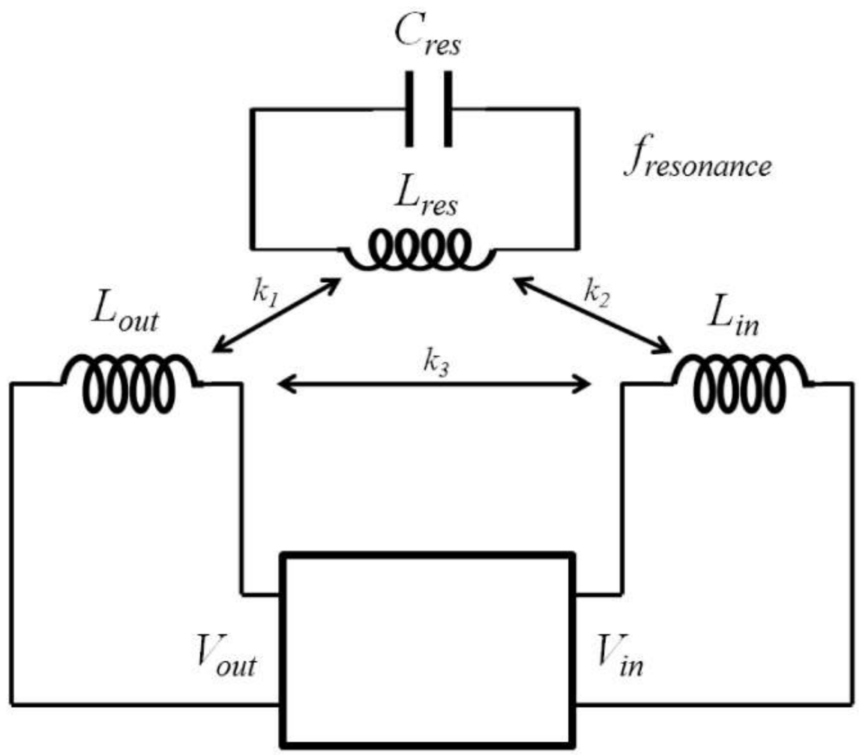

Figure 20: Primary and secondary resonant circuits.

The road embedded units are made of supply units as shown in Figure 21. This method eliminates the usage of power switches for the energy transition between consecutive rail units because the units independently observe secondary resonance and generate an output synchronized to secondary resonance, as illustrated in Figure 22. The transition technic between units also eliminates the complex control mechanisms required to manage energy transitions.

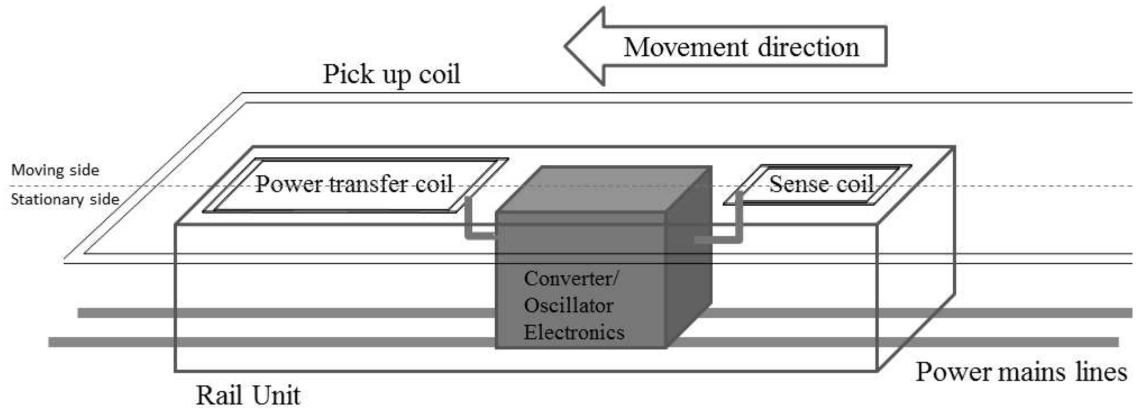

Figure 21: Structure of rail unit.

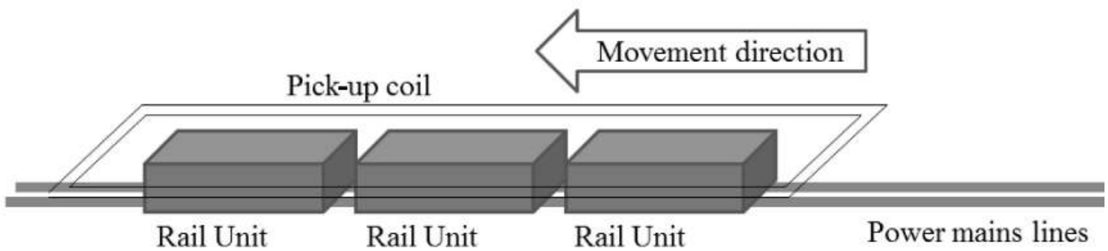

Figure 22: Method of power switch elimination.

There are several advantages of the proposed method. The output coil can be designed only for coupling, so there is no need for resonance approximation. The rail units may be designed for wide-range frequency because of no need to work with a fixed frequency. Non-interoperability issues of the secondary dependence on primary resonance can be addressed due to the frequency independence of the proposed method. It is possible to design such systems as highly efficient WPT systems with primary inductiveness and secondary resonance [3].

Figure 23 illustrates two use cases. On a rail unit, only one coil may be used as the power transfer and sense coils. The coupling factor between adjacent power coils is set up at a low value that they will not trigger to start each other. The absence of a unit due to a failure or maintenance can be tolerated, and the system does not interrupt the roadway. It can be designed for easy replacement to shorten maintenance time. An authorizing signal through a communication line is needed to enable a rail unit to work when it comes to its turn. A central management unit provides the authorizing signal; the signal can be connected to a payment way.

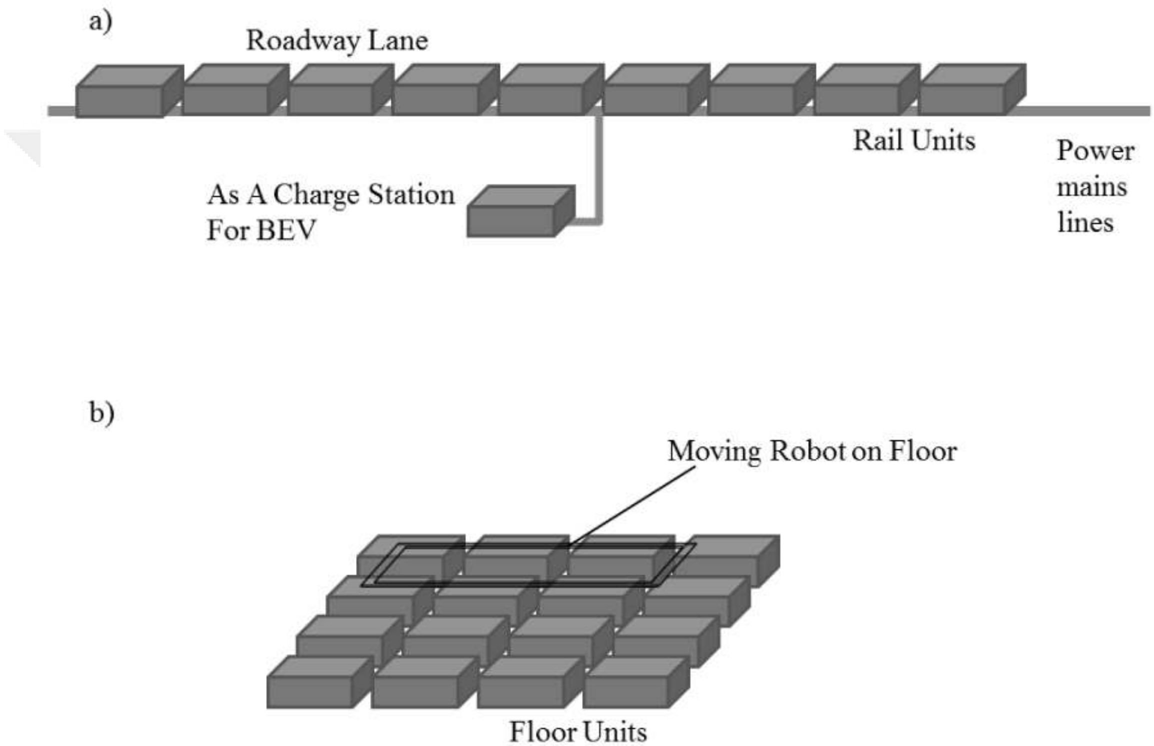

Figure 23: Use cases: (a) Same modules can be used as both rail units or stationary wireless chargers for battery electric vehicles. (b) usage on a two-dimensional floor system.

3.2 Proof of Concept

A simulation of such a system is designed in LTspice for proof of concept. Two adjacent transmit coils are used as rail units. A pick-up coil is assumed as a moving object. The schematic is shown in Figure 24 where the moving object that includes the inductor L1 can move on the rail units that include L2 and L3. On the inactive power transfer coil (L3), a voltage (Vtx2) will be induced by the magnetic field of the receiving coil (L1) related to its current, which is dependent on the load (R1) which represents the vehicle's consumption. In the case of movement of the object (L1) in a direction from the active transmitting coil (L2) to the inactive one (L3), the coupling factor between receiving coil (L1) and transmitting coils will change based on their distance. The induced voltage on the inactive transmitting coil increases during the movement. This voltage is used for sensing the receiving coil's existence. The resonance frequency of the system's secondary can be measured by either an analog measurement circuit or digitally by an algorithm.

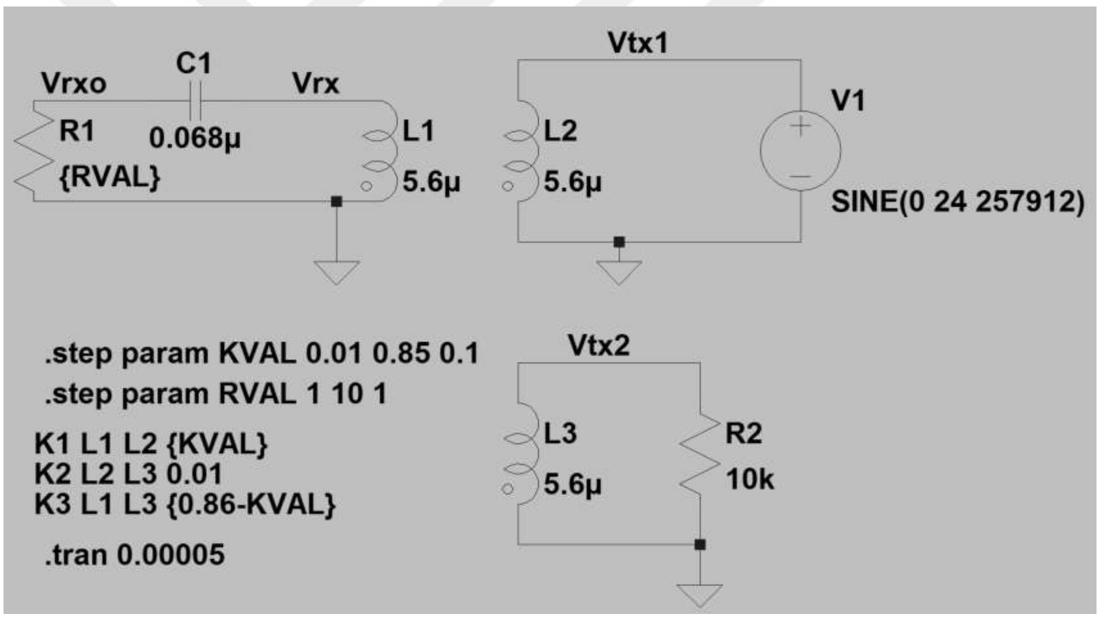

Figure 24: Schematic of the LTspice simulation.

Simulation results revealed the dependency of induced voltage (Vtx2 in Figure 24) on the inactive transmitting coil to both the load changes and the movement of receiving coil. A magnetic field is generated by L1 related to its load current. The load current can be adjusted by varying R1. RVAL is the parametric value of R1 changing from 1 Ohm to 10 Ohm. When the load current flows on R1 increases, RVAL decreases; however, the magnetic field and induced voltage (Vtx2) increase. If

RVAL increases, the load current on R1 decreases, and induced voltage Vtx2 on L3 drops. On the other hand, the coupling factor between L1 and L2 is parameterized by KVAL, representing the movement of L1 in the direction from L2 to L3 on the x-axis. When L1 moves towards L3, KVAL decreases but the coupling factor between L1 and L3 increases. When L1 is at the middle position between L2 and L3, the induced voltage Vtx2 on L3 becomes the maximum. This phenomenon is shown as a dark red color in Figure 25. Therefore, it is possible to trigger the next rail unit by sensing the magnetic field of the moving pick-up coil. Figure 25 also shows where the optimum position points are on the x-axis and values of Vtx2 for triggering transitions from one rail unit to another.

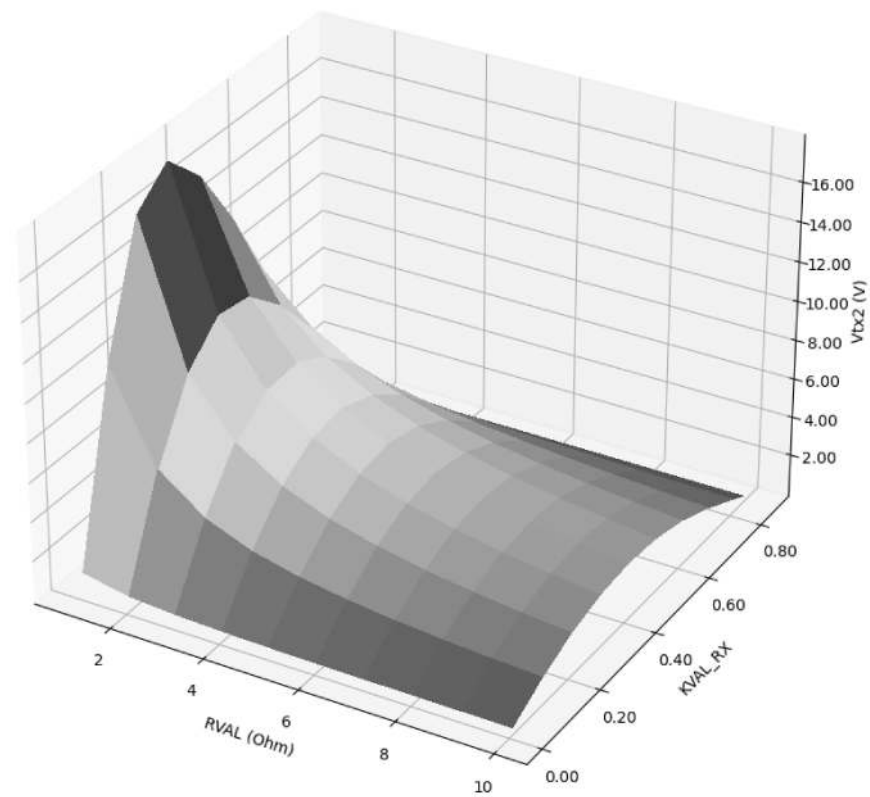

Figure 25: Load and coupling factor dependencies of Vtx2.

The experimental study of the proposed idea of "the primary tracks the secondary resonance method" is conducted in the laboratory. The experimental setup is shown in

Figure 26 and Figure 27. The experiment compares the simulation results by LTspice and measurement results from the lab. The pick-up coil (receiving) is mounted on the x-axis of a 3-dimensional cartesian machine. The pick-up coil marked as L1 in Figure 27 can move on the x-axis by 0.1mm steps in the movement directions as marked. The rail units are realized by commercially available coils marked as L2 and L3 in Figure 27. The measurement setup consists of an oscilloscope, a signal generator, and a power amplifier. The power amplifier is fed by a signal generator and drives L2. The oscilloscope measures voltages on L2 and L3. The L1 coil is loaded with LEDs. L1 coil moved in X-direction by the cartesian machine with 5mm steps. In the initial position, L1 covers only L2. In the initial position, L1 covers only L2. Vtx2 voltage on L3 is only generated by magnetic coupling between L2 and L3. The movement of L1 with the cartesian machine in the X-axis covers both L2 and L3. When L1 is loaded, a current flows in it related to its load. This current generates a voltage on L3 during the coverage of both L2 and L3. The induced voltage on L3, Vtx2, measured with the positions. The voltage of Vtx2 is shown in Figure 28.

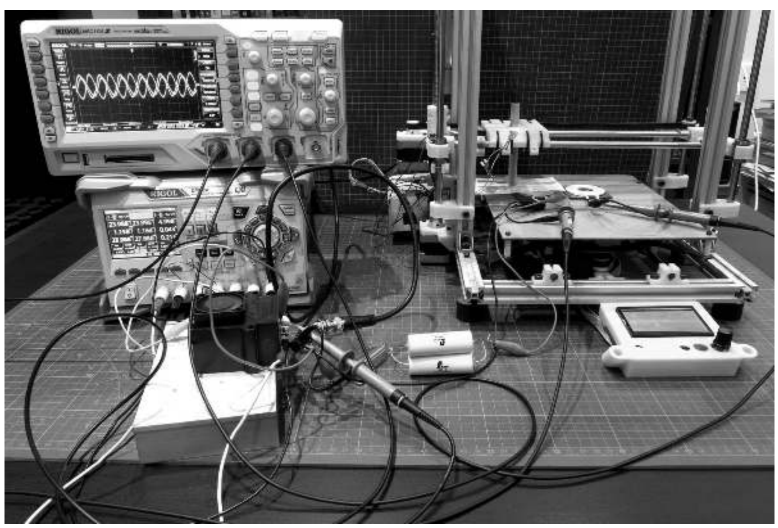

Figure 26: Setup which is used for proof of concept and measurements between stationary coils and moving coil.

Pick-up coil is attached to a moving head of a cartesian placement machine as shown in Figure 27.

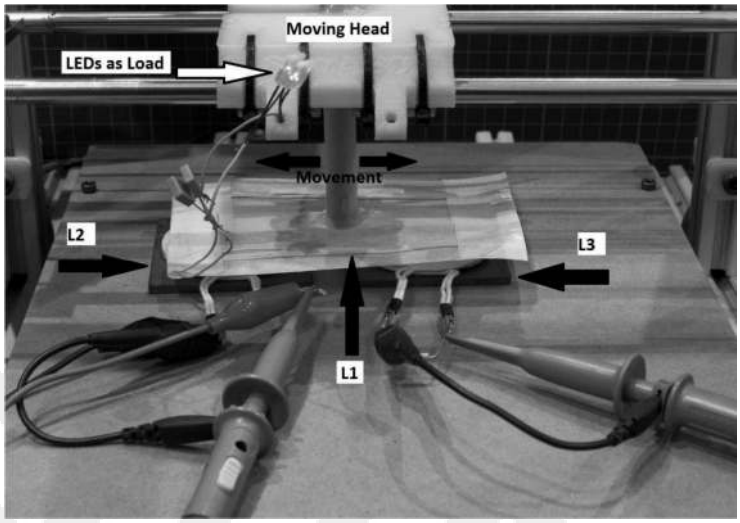

Figure 27: Close view of the measurement setup.

L2 and L3 are planar spiral coils on square-shaped ferrites. They are off-the-shelf parts. The coils are 53mm by 53mm. There is a 12mm distance between them. In this situation, the positions of 60mm and 65mm in Figure 28 are the positions of the moving head where the induced voltage on L3 is maximum. To illustrate the experimental setup visually, Figure 27 shows the L1 coil when the voltage on L3 is at its maximum. The explained setup above is a proof of concept that it is possible to induce a voltage on an inactive transmit coil for sensing and triggering the start-up of the next adjacent power module. The experimental study results can be interpreted as the same as explained before for the Ltspice simulation. If the L3 is triggered and started to transmit power to the L1, the L1 is energized by both transmitter coils of L2 and L3. In this way, L1 smoothly transfers power to the rectifier circuits of the vehicle.

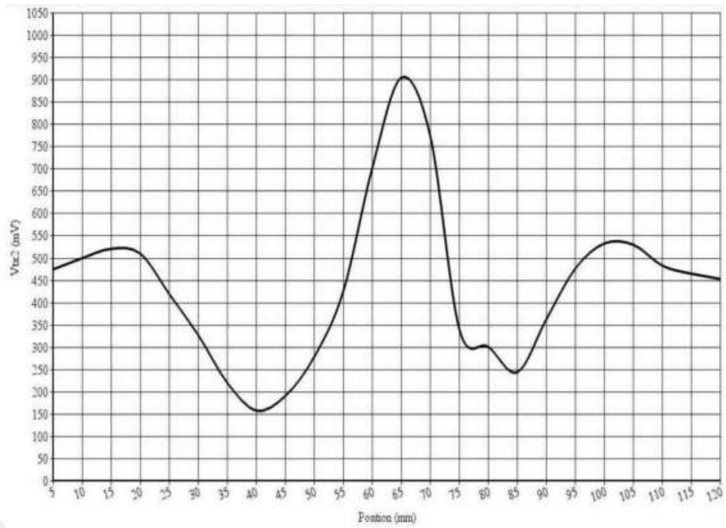

Figure 28: Measurement results, voltage on inactive transmitter coil (V_{tx2}) related to position of receiver coil.

3.3 Magnetic Model and Simulations

One of the topics in this article is to examine the interaction between the transmitting and receiving coils and how the power sent to the receiving coils varies with the vehicle's movement. For this purpose, a system model was built, and simulations were performed in the Ansys Maxwell environment. The dimensions of the coils used in the model are the same as those of the ready-made coils used in the experimental study. The properties of the ferrite and steel parts of the model are the same as the ready-made coil. The length of the receiving coil is the length of the two transmitting coils. Each coil consists of copper windings, ferrite, and steel parts in the order of layers. Figure 29 shows a model built in this way. The upper part (RX) represents the receiving coil or the vehicle, and the three lower parts (TX1, TX2, TX3) represent the transmitting coils or the structure embedded in the path. TX1 and TX2 are active transmit coil, and TX3 is inactive. TX1 and TX2 transmit power. The figure shows the receiving coil's stationary state at the path's starting position. The component produced from this magnetic model was added to the schematic for use in electronic simulations.

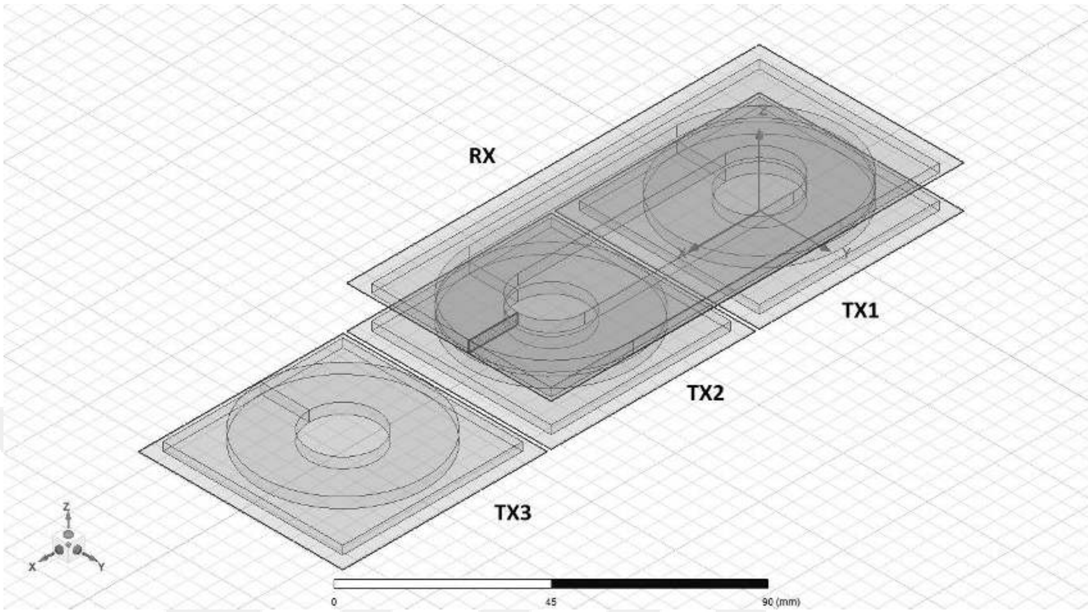

Figure 29: Coil structures of the model of the system.

The schematic of the electrical model of the same system is shown in Figure 30. Winding 1 and 2 represent TX1 and TX2, active transmit coils driven by 48V, 125kHz sources. Winding 3 means TX3, which is the inactive coil. Winding 4 represents RX.

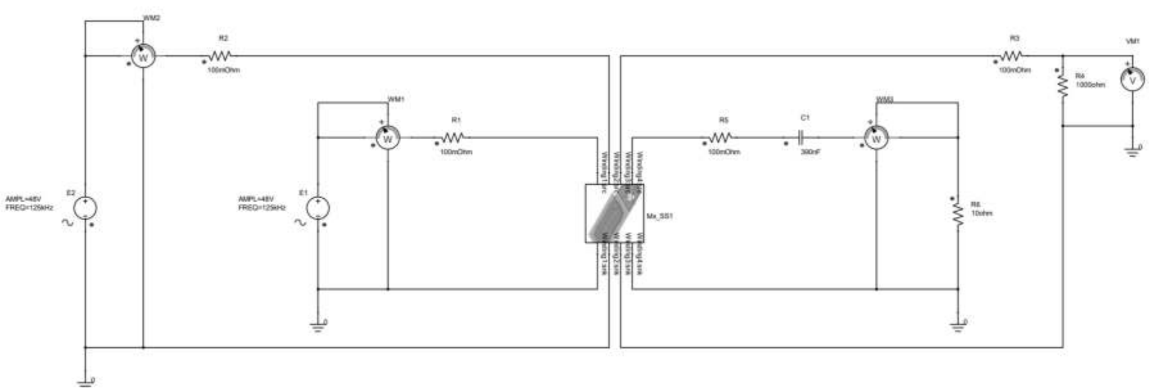

Figure 30: Schematic of the combined model of the system.

The simulations were performed on the established model in the frequency range from 50kHz to 300kHz. The simulations were performed by parametrically varying the distance on the z-axis between the receiving and transmitting coils from 1mm to 5mm in 1mm increments. The simulation results, inductance values, and coupling coefficients are presented in Table 2 and Table 3.

Table 2: Mutual inductance and coupling coefficient between RX and TX1 at 125kHz.

Distance	**1mm**	**5mm**
LTX1 Inductance (uH)	9.770	7.618
LRX Inductance (uH)	6.418	5.029
M Mutual Inductance (uH)	3.628	2.280
k Coupling Coefficient	0.458	0.368

Table 3: Mutual inductance and coupling coefficient between RX and TX3 at 125kHz.

Distance	**1mm**	**5mm**
LTX3 Inductance (uH)	5.921	5.977
LRX Inductance (uH)	6.418	5.029
M Mutual Inductance (uH)	0.118	0.120
k Coupling Coefficient	0.019	0.021

To simulate the vehicle's movement on the road, the position of the receiver coil on the x-axis was changed parametrically in the range of 0mm to 62.5mm in 4 steps. Observing the behavior of the vectors of the magnetic field falling on the coil of the inactive transmitter helps to understand the phenomena during the vehicle's movement. Figure 53 shows B field vectors on the coils during the movement of the receiver coil on the transmitter coils.

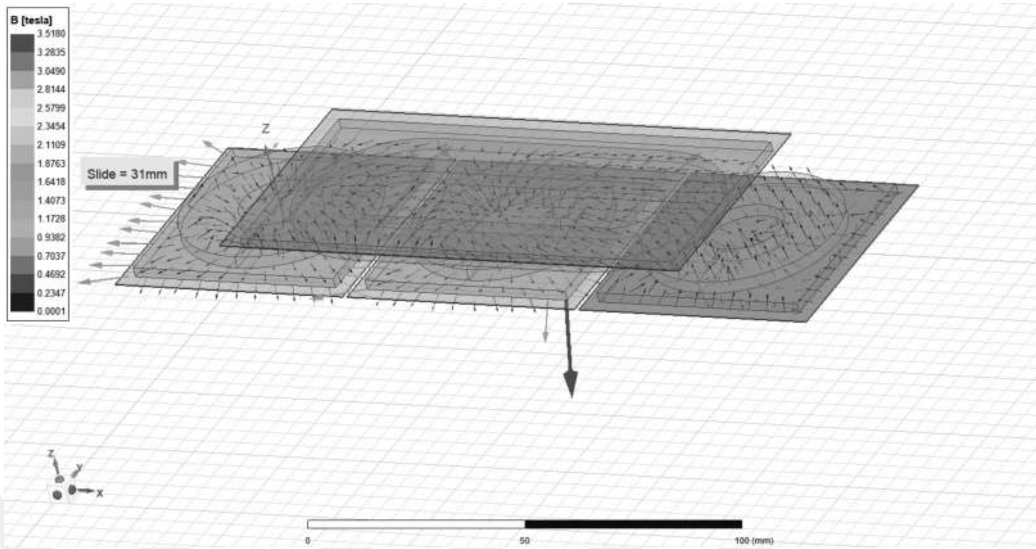

Figure 31: B field vectors on the coils during the movement of receiver coil on transmitter coils.

It has been investigated how the inductances change with the movement of the receiver coil on the x-axis. Due to the presence of another ferrite part (vehicle) moving on the transmitter coils, the inductance value of the transmitter coils changes with the receiver's position. The inductance value of the receiving coil remains constant as seen in Figure 32.

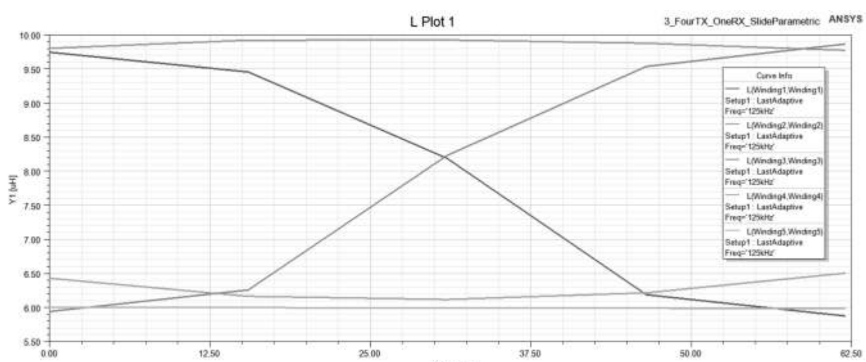

Figure 32: Inductances of the coils versus position of moving receiver coil. With ferrites.

The voltage induced in the inactive transmitter during the receiver's transition from transmitter to transmitter in the x-axis is shown in Figure 33. In the inactive transmitter, it has been examined from which position of the receiver the voltage can be observed, Figure 34.

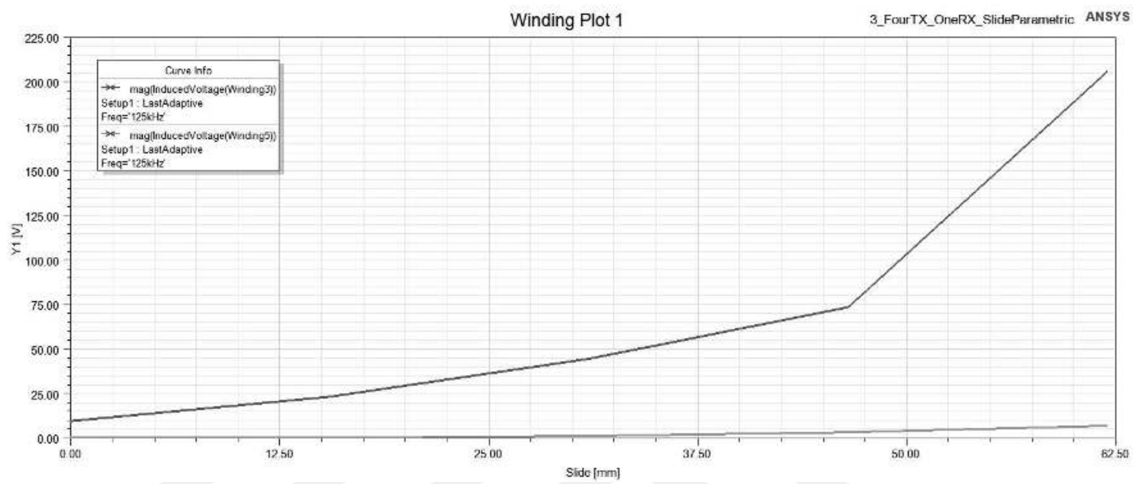

Figure 33: Induced voltage of the coils versus position of moving receiver coil. With ferrites.

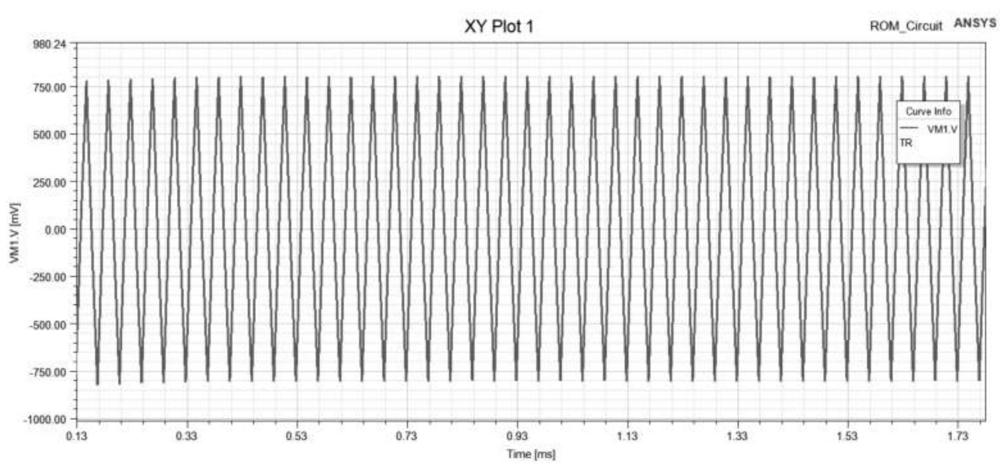

Figure 34: Induced voltage of inactive transmit coil.

It has been seen by simulation that the power transmitted to the receiver varies linearly between two extremes above and below an average value, depending on the receiver's position. Figure 35 shows the simulation result. An equation can be established according to the graph to calculate the effective value of such a changing power value according to the position.

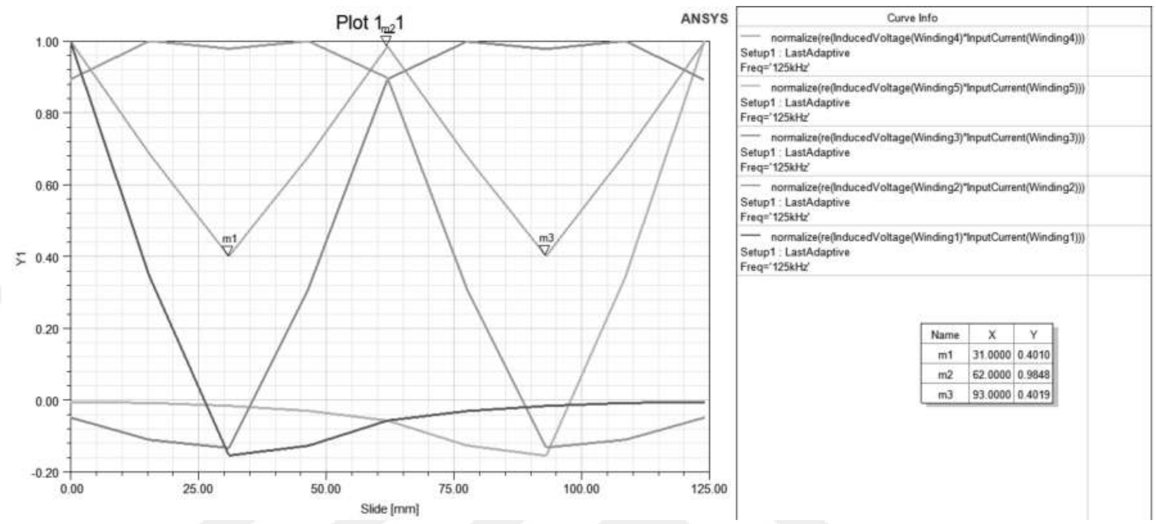

Figure 35: Power of the coils versus position of moving receiver coil while gap is 5mm.

The variation of the transmitted power with frequency and the power values transmitted from the transmitters at 125kHz resonance frequency and transferred to the load on the receiving side is shown in Figure 36. The efficiency is 92 percent.

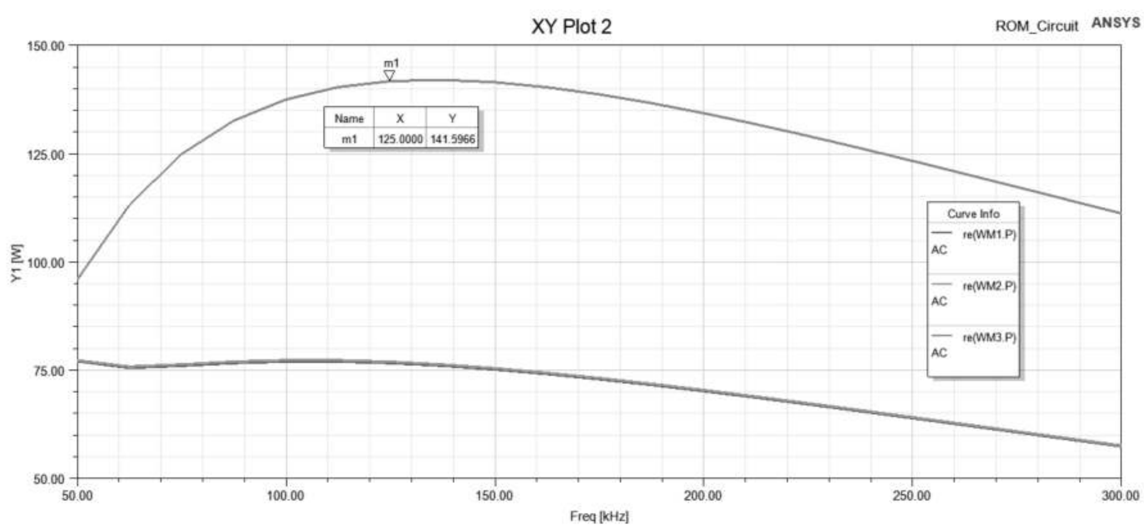

Figure 36: Power of the coils versus frequency.

CHAPTER IV

EXPERIMENT OF PROPOSED WPT SYSTEM FOR LANE MOVING ROBOTS

A coil with part code 760308102142 from Würth Electronics is chosen, and five of them are used for the experimental study. This coil is designed for wireless power transfer applications. The company's 36003600S part code steel material is used for the magnetic shield.

The receiving coil was designed using two off-the-shelf coil materials. Figure 37 shows designed receive coil. It is made as five windings using the materials of two coils.

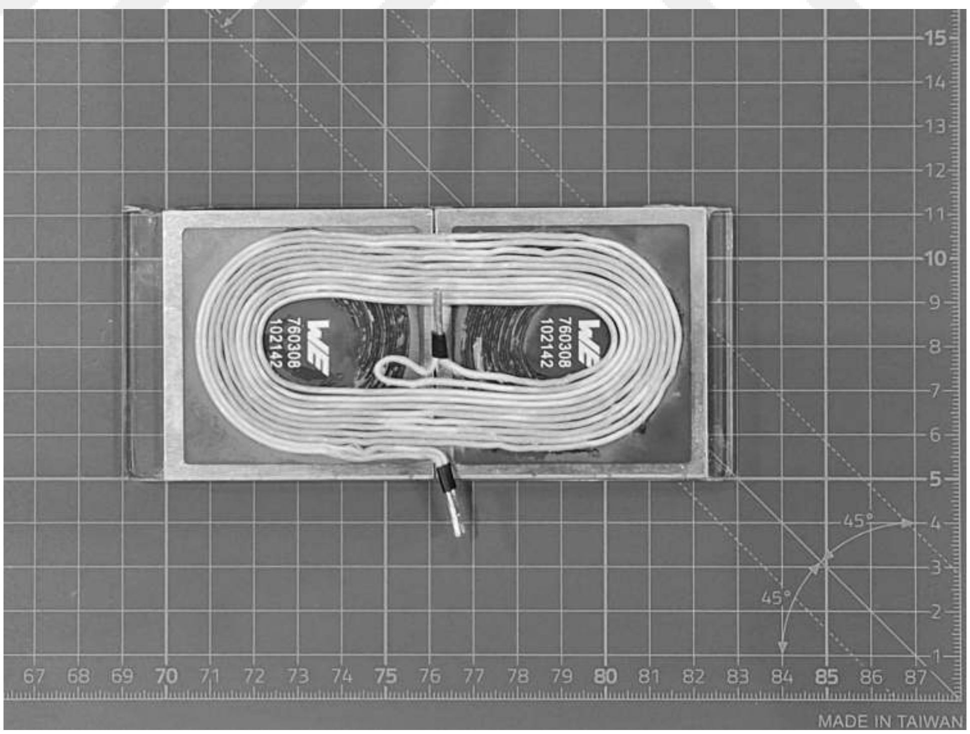

Figure 37: Picture of pick-up coil.

Digilent Analog Discovery 2 and its companion software Waveforms measure the inductive values and coupling factors of the coils. It is a multi-functional tool for laboratories. It includes an impedance analyzer for these measurements. The magnetical simulation of the system was made on Ansys Maxwell by the gap range between 1mm to 5mm. For comparison, measurements can be done at two ends of the gap range, 1mm and 5mm. The measurement setup is prepared for 1mm and 5mm. And measurements are taken for 1mm gap and 5mm gap. Figure 38 shows the picture of the measurement setup for inductance values and coupling coefficients of the coils at 1mm gap.

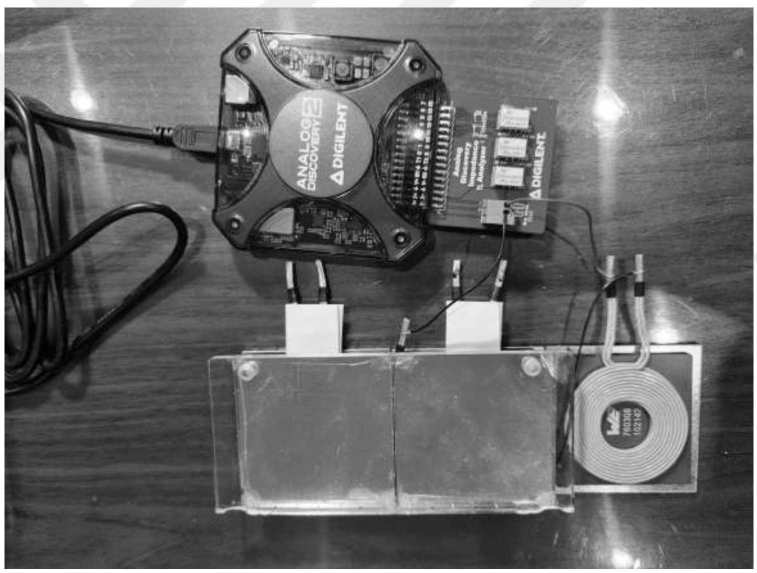

Figure 38: Measurement set-up for inductances and coupling coefficients of the coils at 1mm gap.

Side view of measurement set-up for inductances and coupling coefficients of the coils at 1mm gap, Figure 39 and at 5mm gap, Figure 40.

Figure 39: Side view of measurement set-up.

Figure 40: Side view of measurement set-up.

Inductance values of the coils are measured in a frequency range between 50kHz and 1MHz to see the effect of frequency change on inductance values. Figure 41 shows a screenshot of Waveforms software impedance analyzer and inductance of pick-up coil versus frequency. And Figure 42 shows a screenshot of Waveforms software inductance-meter and inductance of pick-up coil at 125kHz when it is put together with TX coils by the gap is 5mm.

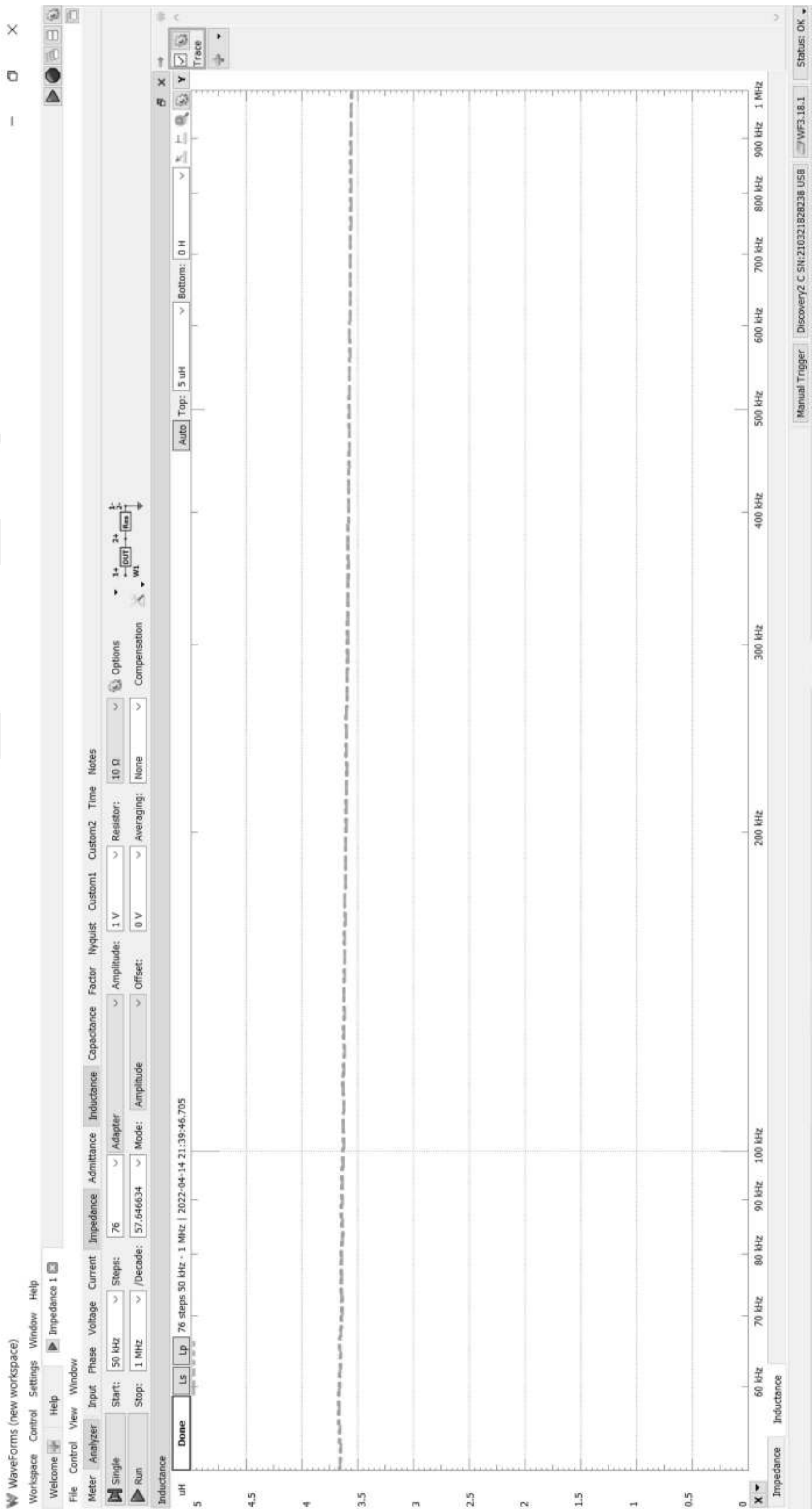

Figure 41: Waveforms software and inductance of pick-up coil vs frequency.

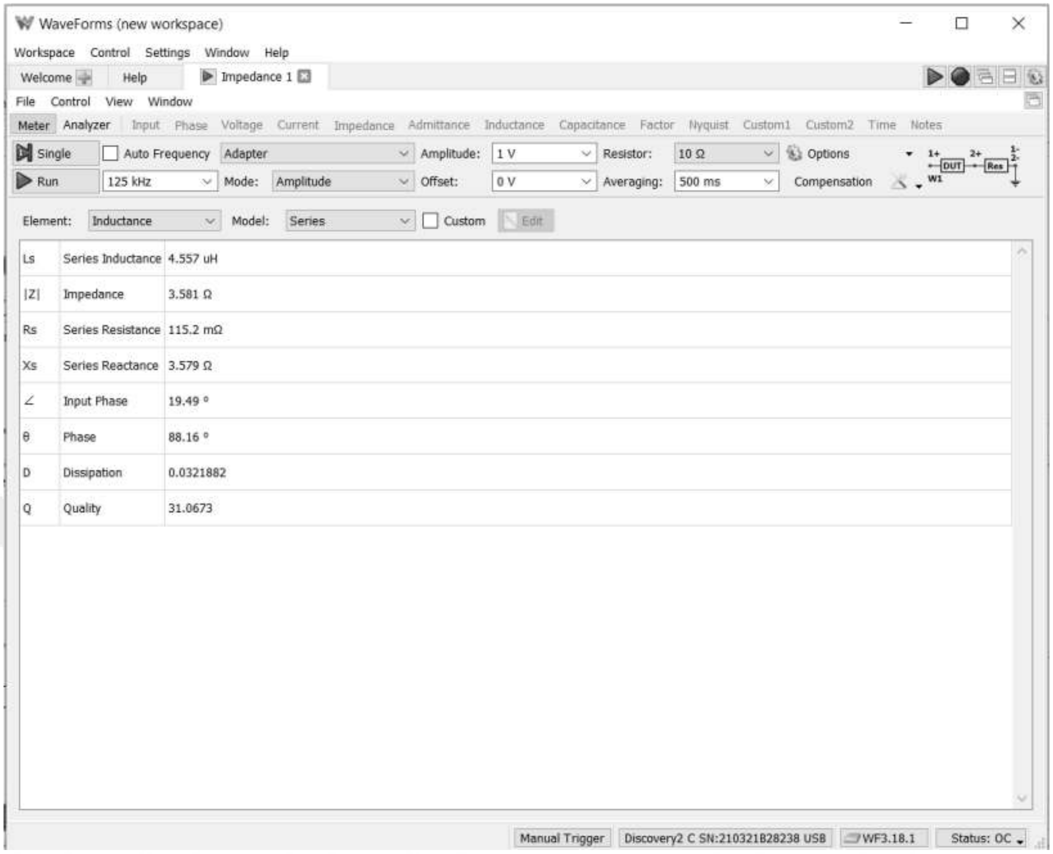

Figure 42: Inductance measurement of pick-up coil at 125kHz and at 5mm gap.

Table 4 and Table 5 shows the measured values of the pick-up and transmitter coil at 125kHz with a 1mm gap and 5mm gap between the pick-up coil and transmitter coils.

Table 4: Measured values of pick-up coil at 125kHz.

Distance	**1mm**	**5mm**	**Standalone**
Ls Series Inductance (uH)	5.824	4.530	3.619
|Z| Impedance (Ω)	4.576	3.559	2.843
Rs Series Resistance (mΩ)	139.6	112.0	80.68
Xs Series Reactance (Ω)	4.574	3.558	2.842
∠ Input Phase (°)	24.28	19.39	15.75
θ Phase (°)	88.25	88.20	88.37
D Dissipation	0.0305	0.0315	0.0284
Q Quality	32.77	31.78	35.22

Table 5: Measured values of transmitter coil at 125kHz.

Distance	**1mm**	**5mm**
Ls Series Inductance (uH)	9.048	6.948
|Z| Impedance (Ω)	7.109	5.459
Rs Series Resistance (mΩ)	179.0	132.3
Xs Series Reactance (Ω)	7.107	5.457
∠ Input Phase (°)	34.93	28.31
θ Phase (°)	88.56	88.61
D Dissipation	0.0252	0.0242
Q Quality	39.69	41.26

Coupling coefficients between transmitter coils (TX1, TX2, TX3) and pick-up coil (RX) can be calculated through measured mutual inductances for each gap distance, 1mm and 5mm. Well-known mutual inductance with dot convention method is used. According to this method, inductances are known separately and have a joint magnetic field. The beginning of winding of each coil is marked with a dot, and two measurements of total inductances will be taken when coils are serially connected with the dots on the same side and the dots on the opposite sides. Two equations, Equation 2, Equation 3 help us to calculate mutual inductance M, where LT1 total inductance for the first measurement, LT2 total inductance for the second measurement.

$$LT1 = L1 + L2 - 2M \tag{2}$$

$$LT2 = L1 + L2 + 2M \tag{3}$$

Mutual inductance equation becomes as below.

$$M = \frac{LT2 - LT1}{4} \tag{4}$$

Mutual inductance equation is also known as Equation 5. And coupling coefficient k can be calculated from this equation.

$$M = k\sqrt{L1L2} \tag{5}$$

$$k = \frac{M}{\sqrt{L1L2}} \tag{6}$$

The calculated mutual inductance and coupling coefficient values are given in Table 6 and Table 7.

Table 6: Mutual inductance and coupling coefficient between RX and TX1 at 125kHz.

Distance	**1mm**	**5mm**
LT1 Total Inductance (uH)	8.162	7.538
LT2 Total Inductance (uH)	21.38	15.34
LTX1 Inductance (uH)	9.074	6.983
LRX Inductance (uH)	5.855	4.518
M Mutual Inductance (uH)	3.304	1.950
k Coupling Coefficient	0.453	0.347

Table 7: Mutual inductance and coupling coefficient between RX and TX3 at 125kHz.

Distance	**1mm**	**5mm**
LT1 Total Inductance (uH)	11.605	10.3
LT2 Total Inductance (uH)	11.89	10.71
LTX3 Inductance (uH)	5.750	5.750
LRX Inductance (uH)	5.855	4.518
M Mutual Inductance (uH)	0.071	0.102
k Coupling Coefficient	0.012	0.020

CHAPTER V

COMPARISON OF RESULTS

Firstly seeing the correlation between simulation and experiments is a well beginning point to compare inductance values and coupling coefficients. RX represents receiver or pick-up coil, TX1 represents active transmitter coil, TX3 represents inactive coil in the tables. Table 8 shows the results at a 1mm gap distance between the receiver coil and the active transmitter coil, and Table 9 shows the results at a 5mm gap.

Table 8: Mutual inductance and coupling coefficients between RX and TX1 at 125kHz with 1mm gap.

	Simulation	**Experiment**	**Difference**
LTX1 Inductance (uH)	9.770	9.074	7.12%
LRX Inductance (uH)	6.418	5.855	8.77%
M Mutual Inductance (uH)	3.628	3.304	8.93%
k Coupling Coefficient	0.458	0.453	1.09%

Table 9: Mutual inductance and coupling coefficient between RX and TX1 at 125kHz with 5mm gap.

	Simulation	**Experiment**	**Difference**
LTX1 Inductance (uH)	7.618	6.983	8.34%
LRX Inductance (uH)	5.029	4.518	10.16%
M Mutual Inductance (uH)	2.280	1.950	14.47%
k Coupling Coefficient	0.368	0.347	5.71%

Table 10 shows the results at a 1mm gap distance between the receiver coil and the inactive transmitter coil, and Table 11 shows the results at a 5mm gap.

Table 10: Mutual inductance and coupling coefficient between RX and TX3 at 125kHz with 1mm gap.

	Simulation	**Experiment**	**Difference**
LTX3 Inductance (uH)	5.921	5.750	2.89%
LRX Inductance (uH)	6.418	5.855	8.77%
M Mutual Inductance (uH)	0.118	0.071	39.83%
k Coupling Coefficient	0.019	0.012	36.84%

Table 11: Mutual inductance and coupling coefficient between RX and TX3 at 125kHz with 5mm gap.

	Simulation	**Experiment**	**Difference**
LTX3 Inductance (uH)	5.977	5.750	3.80%
LRX Inductance (uH)	5.029	4.518	10.16%
M Mutual Inductance (uH)	0.120	0.102	15.00%
k Coupling Coefficient	0.021	0.020	4.76%

The differences are below 15 percent in general. The case is excessive, with a gap of 1mm of TX3 results, which are more than general differences, due to mutual inductance measurement.

Another point for comparison is the value of the induced voltage at the two ends of the inactive transmitter coil when the receiver coil is over the TX1 and TX2. In other words, the receiver coil is just next to the inactive transmitter coil. This value is essential because of the decision of trigger level to activate TX3. The first row of Table 12 shows the voltage values.

And the last point for comparison is the position of the receiver coil on the x-axis, where the induced voltage of TX3 is maximum. The place for activating TX3 shall be between the position of the first row of Table 12 and the position of the second row of the table, which are the points just beginning of the voltage sensing and the end of the voltage sensing. The point of activation of the TX3 will be decided by a trigger level to be determined by the voltage values between these two points.

Table 12: Induced voltage on TX3 at 125kHz.

	Simulation	**Experiment**
RX over TX1 and TX2 (mV)	750	550
X-axis position when RX on max point (mm)	62.5	65

The comparison results in the above tables show a good correlation between the simulation and the experiment. Further work can be on the simulation environment only to model the control system and investigate the system in vehicle movement scenarios.

CHAPTER VI

CONCLUSION

This thesis proposes an alternative method of a wireless power transfer system for moving objects. The proposed method is an alternative to known methods, which use long WPT rails and known methods that use large switches to manage the selection of transmitting coil units that transfers energy. The mobile robot on the floor may be the first application area. The main application areas are warehouse, agricultural, and electric vehicles. The simulation results and the experimental setup are discussed. With simulations in Ansys Maxwell and LTspice environments and experimental studies, it was shown that a vehicle's receive coil induces a voltage in an inactive transmit coil embedded in the path while passing over it. This voltage can be used as a trigger to activate the inactive transmitter during the receiver's transition from the transmitter to the transmitter. And it was shown how the power delivered to the receiver changes with the vehicle's motion. The primary side power switching controls can track signals of the secondary side, and the primary can establish synchronization with the resonance of the secondary side, which receives the energy for powering motors on a vehicle. Control modeling of such a system could be a subject of future study. After the model is created in the MATLAB Simulink environment, it can be converted to C software code and transferred to a microcontroller in an embedded system. The microcontroller generates the signals necessary to drive all semiconductor power electronics elements in the system.

APPENDIX A

SIMULATION RESULTS

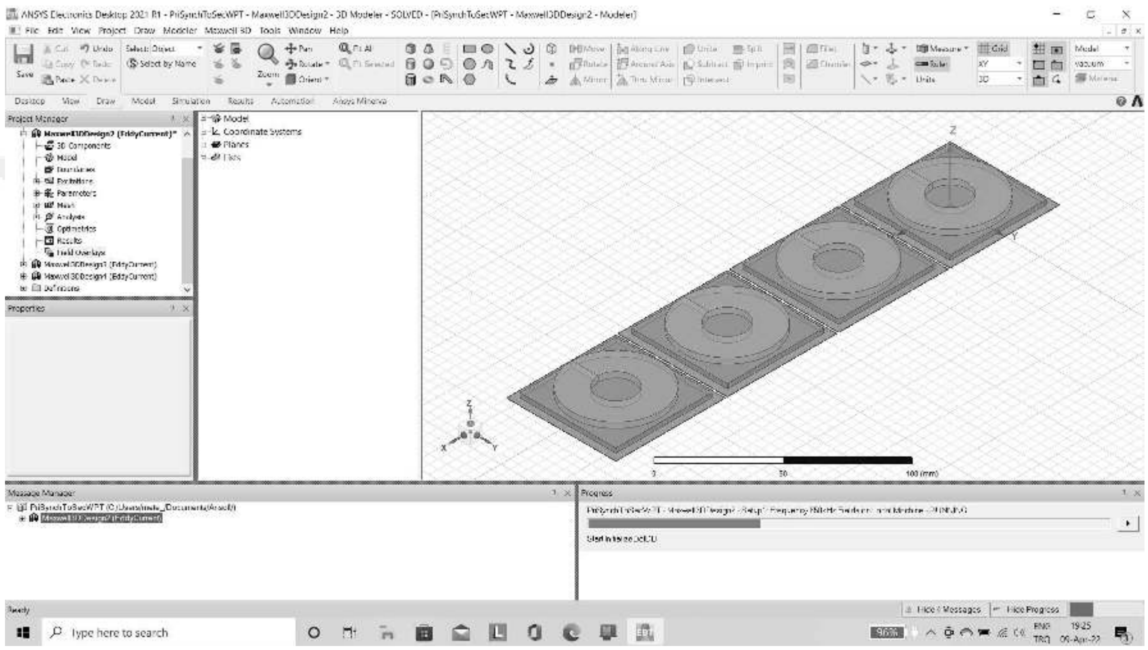

Figure 43: Screenshot of Ansys Maxwell software during the simulation of the system.

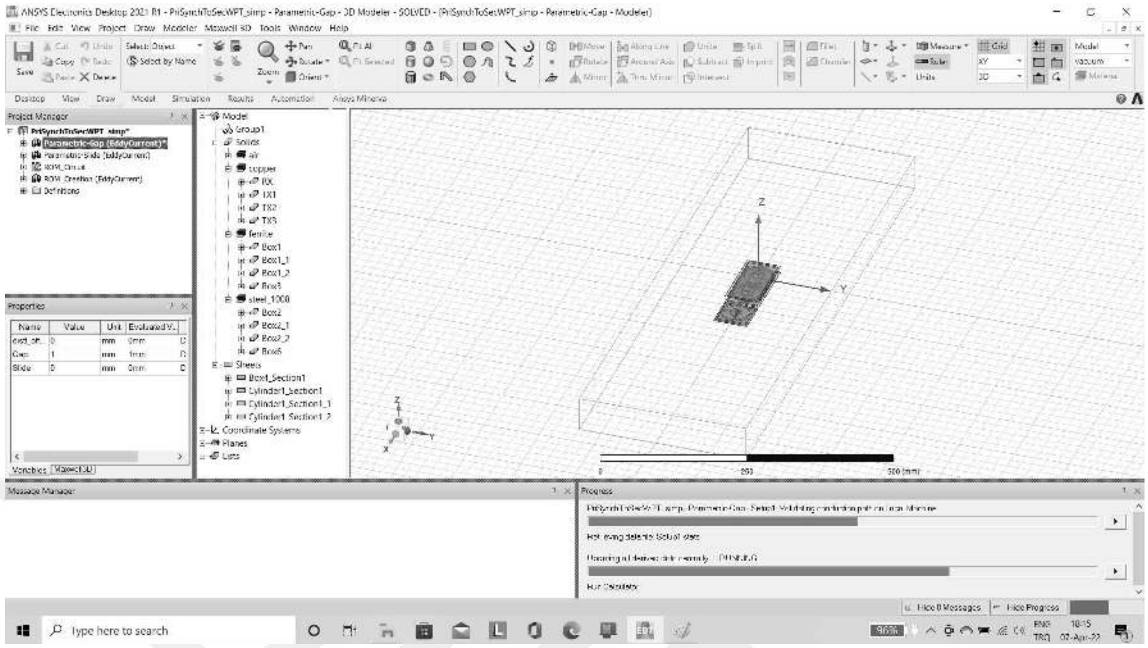

Figure 44: Screenshot of Ansys Maxwell software during the simulation of the system.

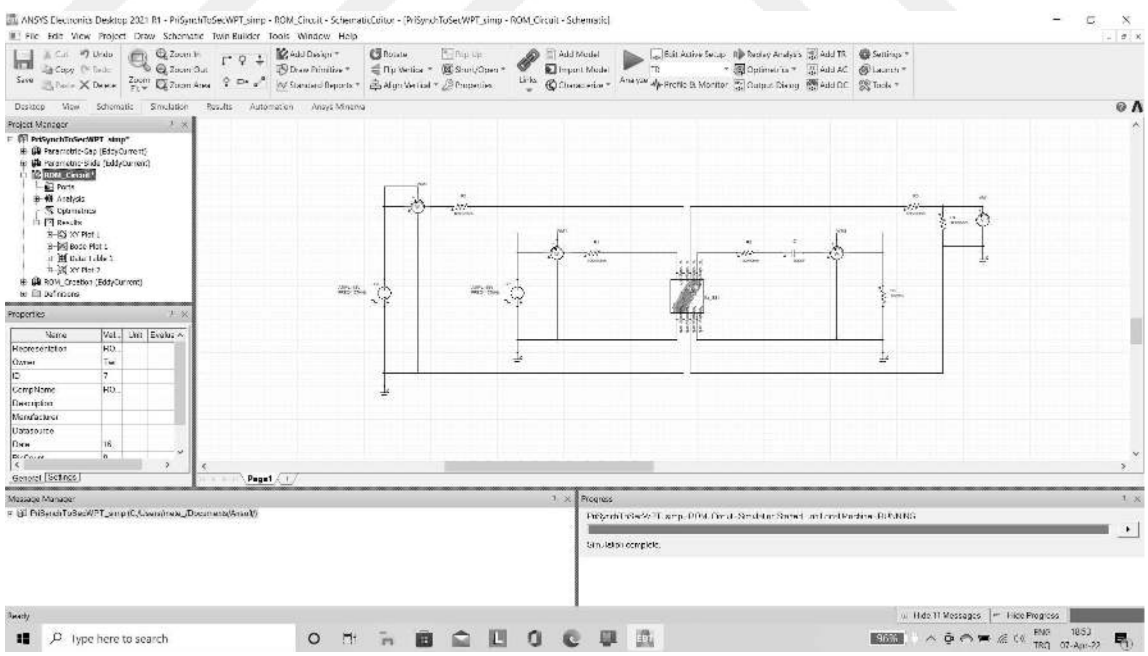

Figure 45: Screenshot of Ansys Maxwell software during the simulation of the system.

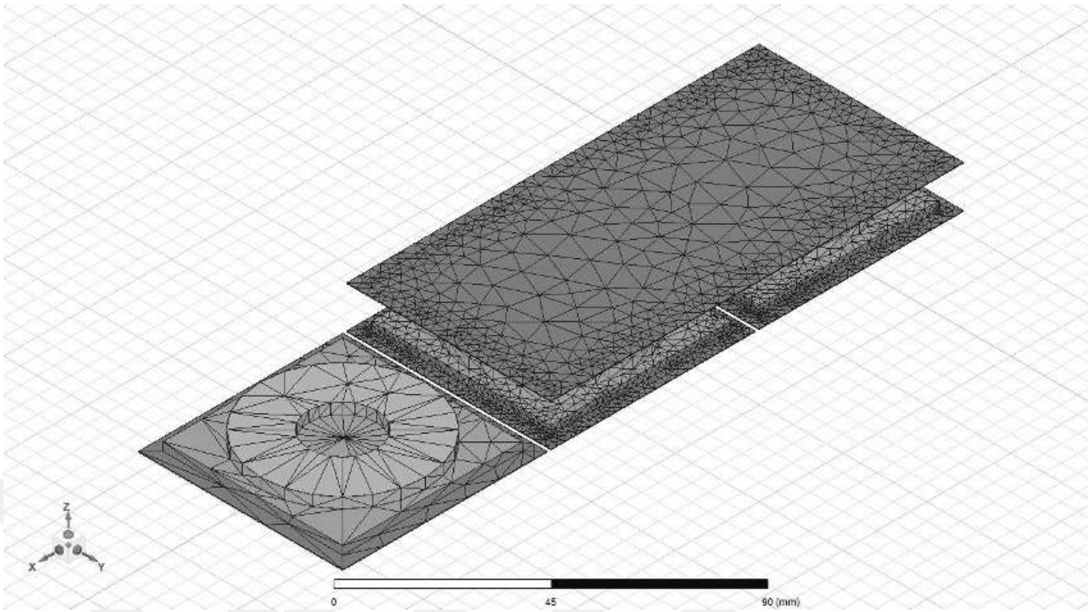

Figure 46: Generated mesh for the calculations of fields on system parts.

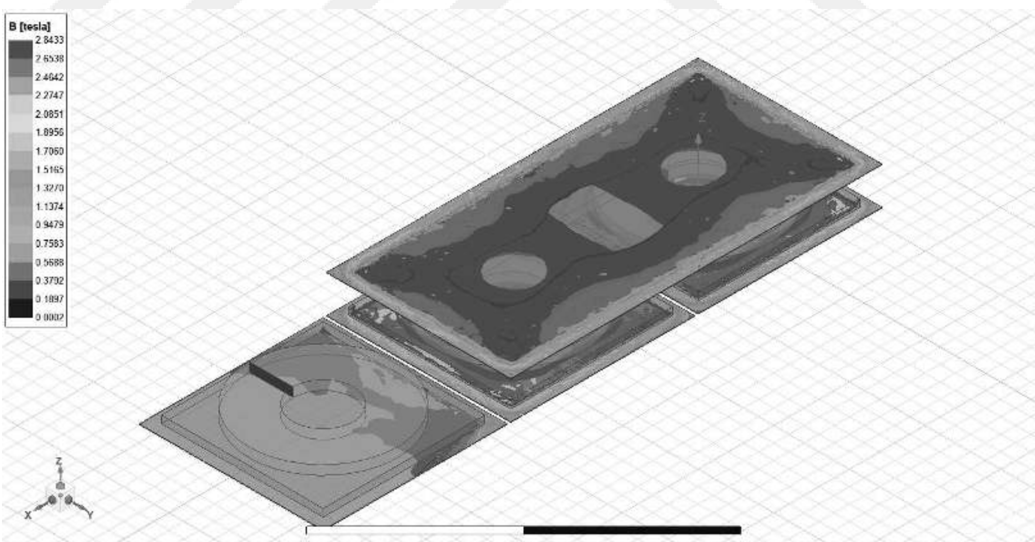

Figure 47: B field on coils.

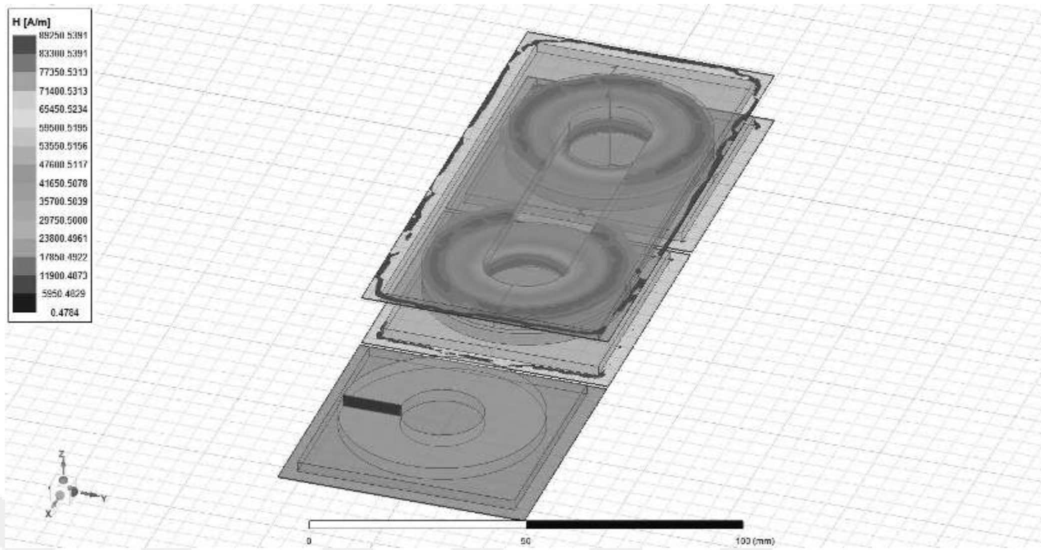

Figure 48: H field on coils.

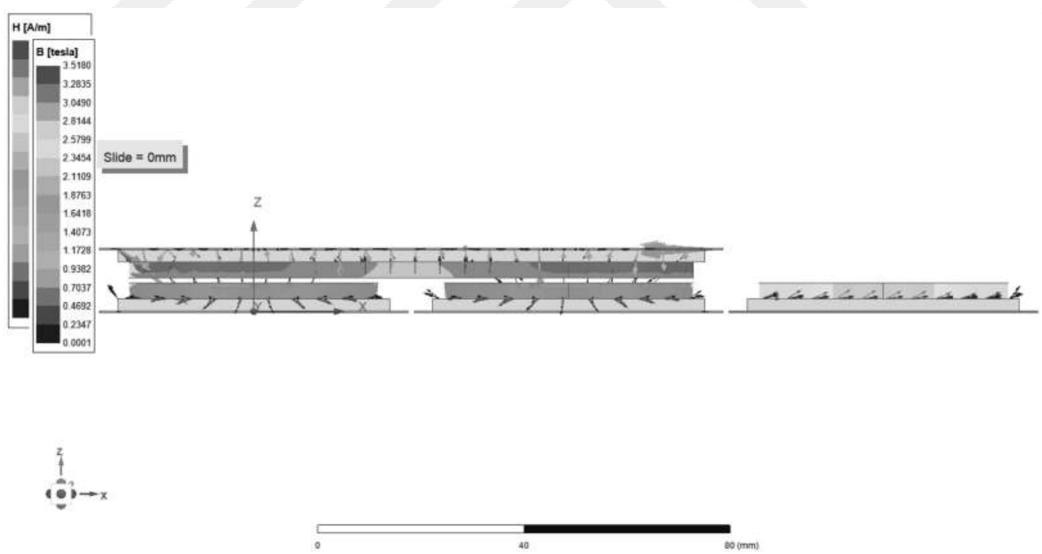

Figure 49: B and H fields on coils versus slide of receiver coil on transmitter coils.

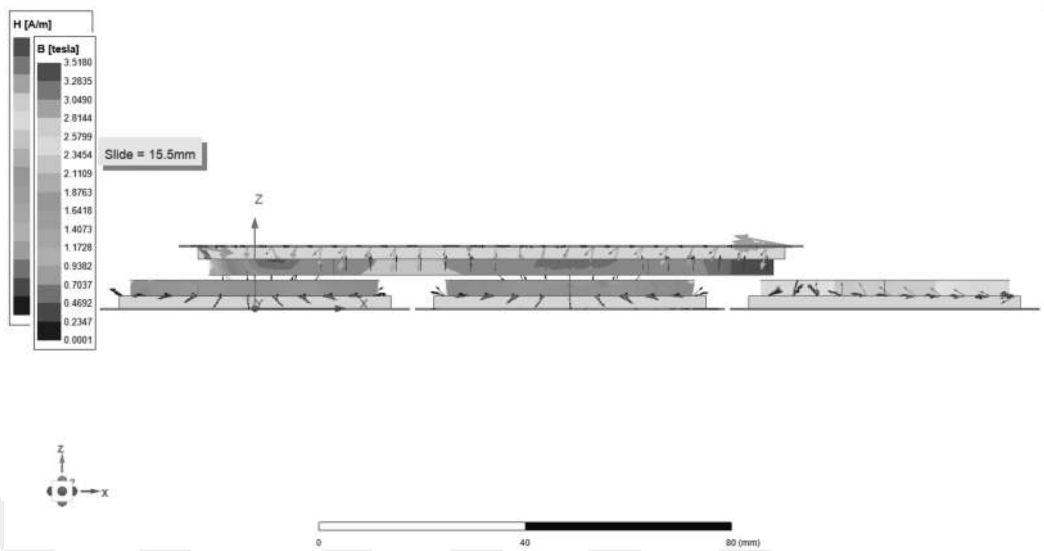

Figure 50: B and H fields on coils versus slide of receiver coil on transmitter coils.

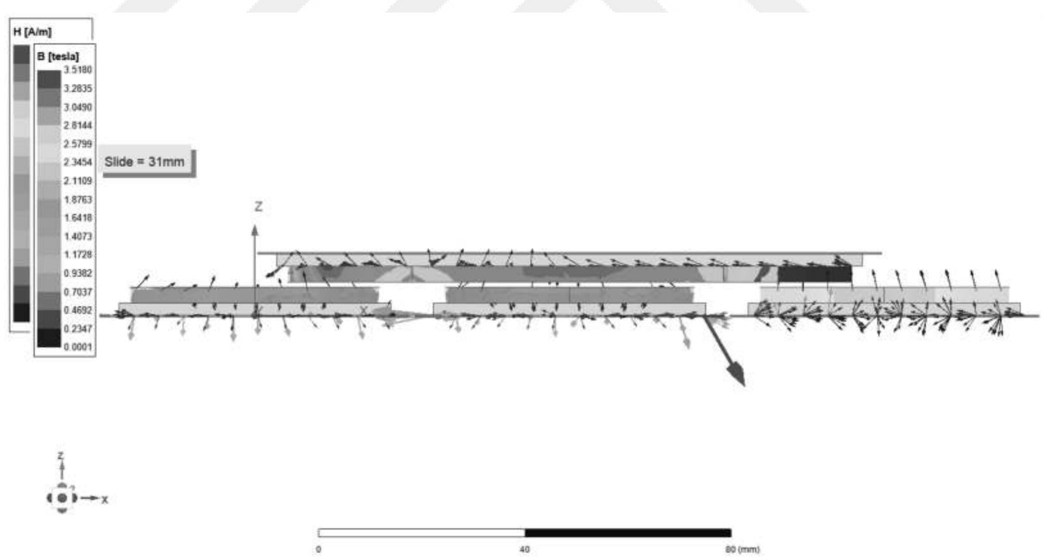

Figure 51: B and H fields on coils versus slide of receiver coil on transmitter coils.

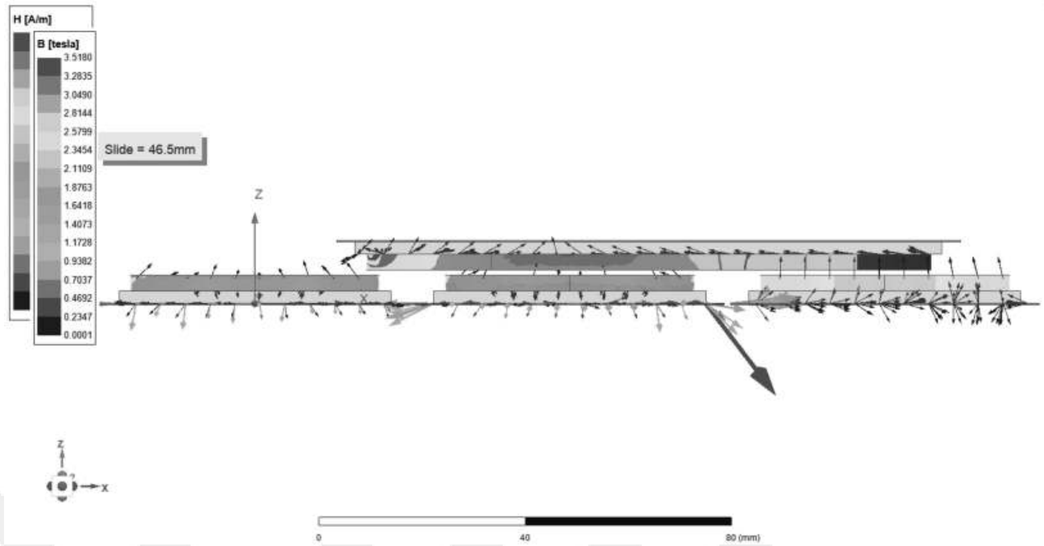

Figure 52: B and H fields on coils versus slide of receiver coil on transmitter coils.

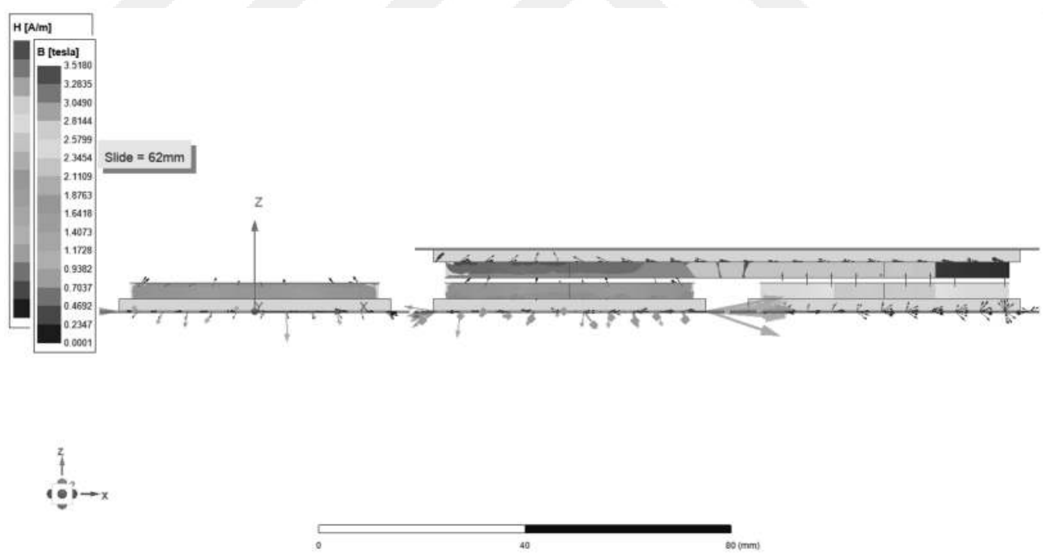

Figure 53: B and H fields on coils versus slide of receiver coil on transmitter coils.

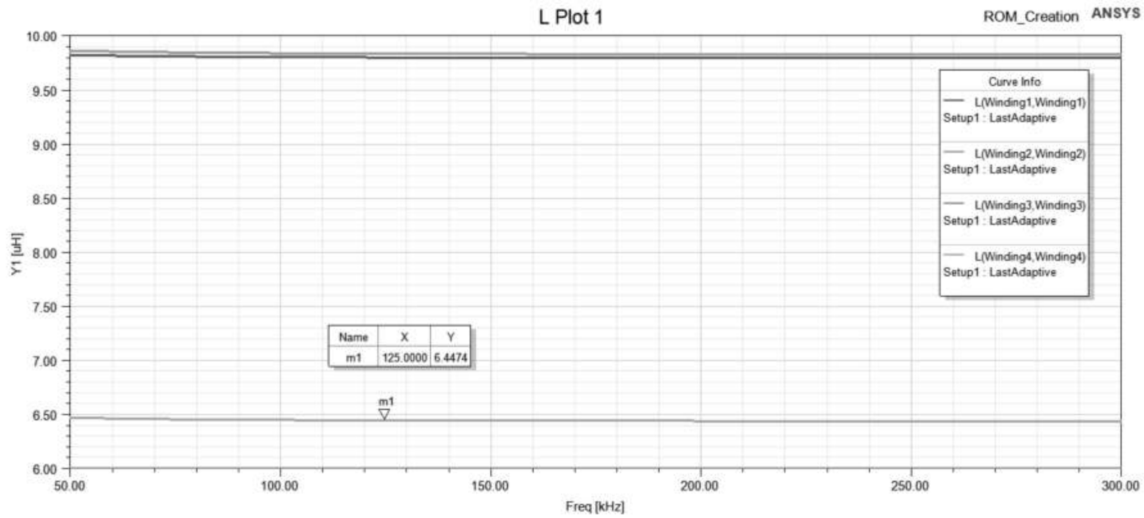

Figure 54: Inductances of the coils versus frequency.

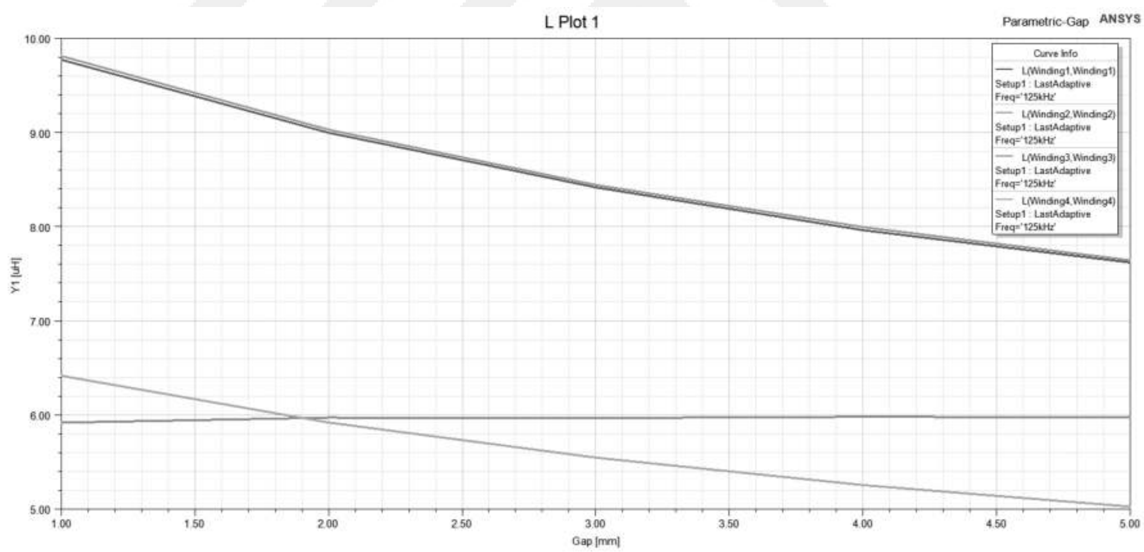

Figure 55: Inductances of the coils versus gap position of moving receiver coil.

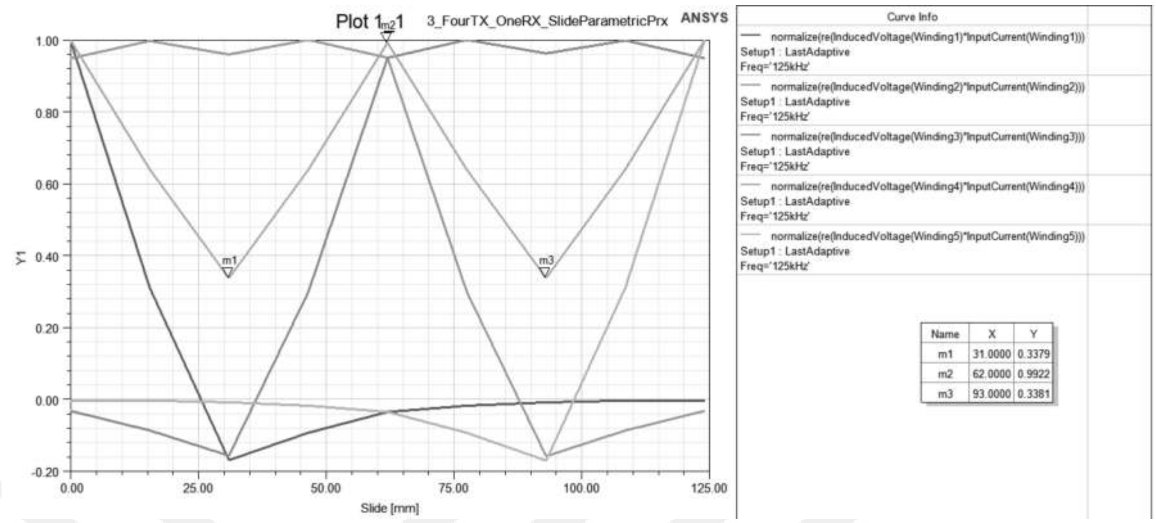

Figure 56: Power of the coils versus position of moving receiver coil while gap is 1mm.

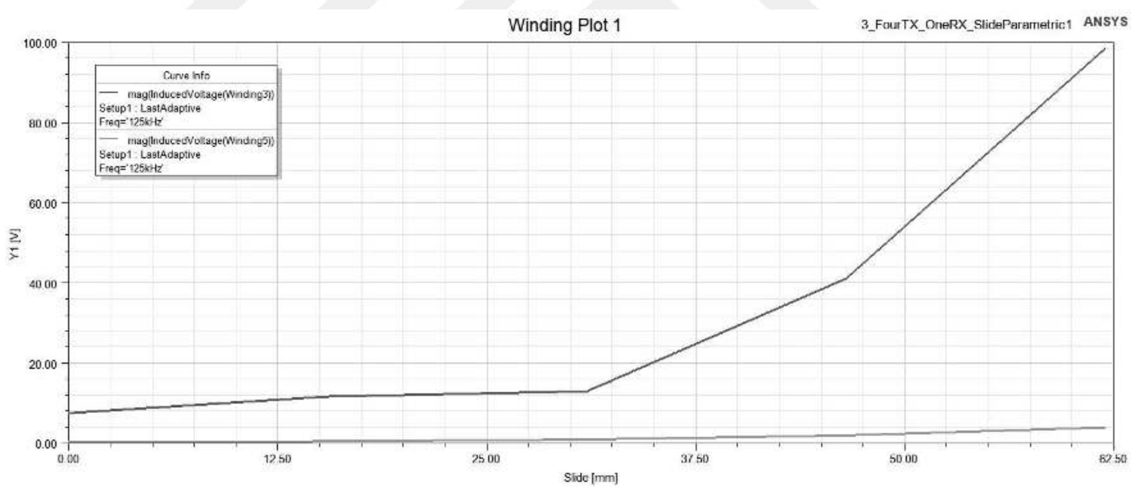

Figure 57: Induced voltage of the coils versus position of moving receiver coil. Without ferrites.

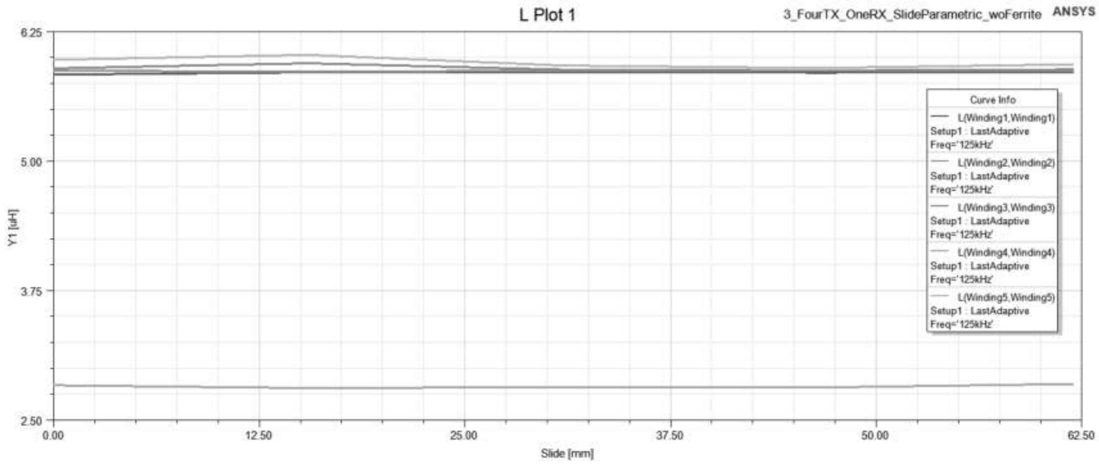

Figure 58: Inductances of the coils versus position of moving receiver coil. Without ferrites.

Bibliography

[1] N. Shinohara, *Wireless Power Transfer via Radiowaves*. ISTE and Wiley, 2014.

[2] M. S. Carmeli, F. Castelli-Dezza, M. Mauri, and G. Foglia, "Contactless energy transmission system for electrical vehicles batteries charging," in *International Conference on Clean Electrical Power (ICCEP)*, pp. 499–505, 2015.

[3] Y. Zhang, *Key technologies of magnetically-coupled resonant wireless power transfer*. Springer, 2017.

[4] C. T. Rim and C. Mi, *Wireless Power Transfer for Electric Vehicles and Mobile Devices*. IEEE Press and Wiley, 2017.

[5] X. Xiao and W. R. L. Whittaker, "Energy considerations for wheeled mobile robots operating on a single battery discharge," Tech. Rep. CMU-RI-TR-14-16, Carnegie Mellon University, Pittsburgh, PA, August 2014.

[6] I. Besselink, P. Oorschot, van, and H. Nijmeijer, "Design of an efficient, low weight battery electric vehicle based on a VW Lupo 3L," in *25th International Battery, Hybrid and Fuel Cell Electric Vehicle Symposium (EVS 25), 5-9 November 2010 Shenzen, China*, (Shenzen, China), 2010.

[7] M. Rozman, *Inductive wireless power transmission for automotive applications*. PhD thesis, 2019.

[8] L. Xie, C. Henkel, K. Stol, and W. Xu, "Power-minimization and energy-reduction autonomous navigation of an omnidirectional mecanum robot via the dynamic window approach local trajectory planning," *International Journal of Advanced Robotic Systems*, vol. 15, no. 1, p. 1729881418754563, 2018.

[9] S. Seok, A. Wang, M. Y. Chuah, D. J. Hyun, J. Lee, D. M. Otten, J. H. Lang, and S. Kim, "Design principles for energy-efficient legged locomotion and implementation on the mit cheetah robot," *IEEE/ASME Transactions on Mechatronics*, vol. 20, no. 3, pp. 1117–1129, 2015.

[10] D. Berjoza and I. Jurgena, "Influence of batteries weight on electric automobile performance," in *16th International Scientific Conference Engineering for Rural Development, 24-25 May 2017 Jelgava, Latvia*, (Jelgava, Latvia), pp. 1388–1394, 2017.

[11] D. Berjoza and I. Jurgena, "Effects of change in the weight of electric vehicles on their performance characteristics," *Agronomy Research*, vol. 15, pp. 952—-963, May 2017.

[12] C. S. Thomas, *Sustainable Transportation Options for the 21st Century and Beyond*. Springer, Cham, 2015.

[13] L. Hutchinson, B. Waterson, B. Anvari, and D. Naberezhnykh, “Potential of wireless power transfer for dynamic charging of electric vehicles,” *IET Intelligent Transport Systems*, vol. 13, no. 1, pp. 3–12, 2019.

[14] L. Patnaik, P. S. Huynh, D. Vincent, and S. S. Williamson, “Wireless opportunity charging as an enabling technology for ev battery size reduction and range extension: Analysis of an urban drive cycle scenario,” in *IEEE PELS Workshop on Emerging Technologies: Wireless Power Transfer (Wow)*, pp. 1–5, 2018.

[15] N. Tesla, “System of electric lighting,” U.S. Patent 454 622, June 23, 1891.

[16] M. Hutin and L. Maurice, “Transformer system for electric railways,” U.S. Patent 527 857, October 23, 1894.

[17] N. Tesla, “Apparatus for transmitting electrical energy,” U.S. Patent 1 119 732, December 1, 1914.

[18] A. Esser and H.-C. Skudelny, “A new approach to power supplies for robots,” *IEEE Transactions on Industry Applications*, vol. 27, no. 5, pp. 872–875, 1991.

[19] J. M. Fernandez and J. A. Borras, “Contactless battery charger with wireless control link,” U.S. Patent 6 184 651, February 6, 2001.

[20] R. Shadid, S. Noghanian, and A. Nejadpak, “A literature survey of wireless power transfer,” in *IEEE International Conference on Electro Information Technology (EIT)*, pp. 0782–0787, 2016.

[21] S. Hekal, A. Allam, A. B. Abdel-Rahman, and R. K. Pokharel, *Compact Size Wireless Power Transfer Using Defected Ground Structures*. Springer, 2019.

[22] W. Corporation, “Witricity acquires qualcomm halo.”

[23] J. I. Agbinya, *Wireless Power Transfer 2nd Edition*. River Publishers, 2016.

[24] N. P. Suh and D. H. Cho, *The On-line Electric Vehicle*. Springer, 2017.

[25] N. Shinohara, ed., *Wireless Power Transfer*. London: The Institution of Engineering and Technology, 2018.

[26] K. Y. Kim, ed., *Wireless Power Transfer – Principles and Engineering Explorations*. Rijeka: InTech, 2011.

[27] K. Song, K. E. Koh, C. Zhu, J. Jiang, C. Wang, and X. Huang, “A review of dynamic wireless power transfer for in-motion electric vehicles,” in *Wireless Power Transfer* (E. Coca, ed.), ch. 6, Rijeka: IntechOpen, 2016.

[28] A. Vadde and B. Sudha, “Enhancement of efficiency for wireless power transfer system using wireless link,” in *International Conference on Circuits and Systems in Digital Enterprise Technology (ICCSDET)*, pp. 1–6, 2018.

[29] D. Kim, A. Abu-Siada, and A. T. Sutinjo, "Application of fra to improve the design and maintenance of wireless power transfer systems," *IEEE Transactions on Instrumentation and Measurement*, vol. 68, no. 11, pp. 4313–4325, 2019.

[30] K. Li, S.-C. Tan, and R. S. Y. Hui, "Single-switch-regulated resonant wpt receiver," *IEEE Transactions on Power Electronics*, vol. 34, no. 11, pp. 10386–10391, 2019.

[31] V.-B. Vu, M. Dahidah, V. Pickert, and V.-T. Phan, "Comparison of single and three phase dynamic charging systems for electric vehicles," in *IEEE PELS Workshop on Emerging Technologies: Wireless Power Transfer (WoW)*, pp. 220–225, 2019.

[32] F. Grazian, P. van Duijsen, T. B. Soeiro, and P. Bauer, "Advantages and tuning of zero voltage switching in a wireless power transfer system," in *IEEE PELS Workshop on Emerging Technologies: Wireless Power Transfer (WoW)*, pp. 367–372, 2019.

[33] V.-B. Vu, M. Dahidah, V. Pickert, and V.-T. Phan, "A concept of multiphase dynamic charging system with constant output power for electric vehicles," in *IEEE PELS Workshop on Emerging Technologies: Wireless Power Transfer (WoW)*, pp. 229–233, 2019.

[34] K. N. Mude, *Wireless Power Transfer for Electric Vehicle*. PhD thesis, University of Padova, Italy, 2014.

[35] A. Karalis, J. Joannopoulos, and M. Soljačić, "Efficient wireless non-radiative mid-range energy transfer," *Annals of Physics*, vol. 323, pp. 34–48, 11 2006.

[36] A. Kurs, A. Karalis, R. A. Moffatt, J. D. Joannopoulos, P. Fisher, and M. Soljaić, "Wireless power transfer via strongly coupled magnetic resonances," *Science*, vol. 317, pp. 83 – 86, 2007.

[37] M. I. of Technology, "Wireless energy transfer," U.S. Patent 7 825 543, December 2, 2010.